**NASA TECHNICAL NOTE**

**NASA TN D-6031**

c.1

NASA TN D-6031

# A TIME-DEPENDENT METHOD FOR CALCULATING SUPERSONIC BLUNT-BODY FLOW FIELDS WITH SHARP CORNERS AND EMBEDDED SHOCK WAVES

*by Richard W. Barnwell*

*Langley Research Center*
*Hampton, Va. 23365*

NATIONAL AERONAUTICS AND SPACE ADMINISTRATION • WASHINGTON, D. C. • NOVEMBER 1970

| | | |
|---|---|---|
| 1. Report No.<br>NASA TN D-6031 | 2. Government Accession No. | 3. Recipient's Catalog No. |
| 4. Title and Subtitle<br>A TIME-DEPENDENT METHOD FOR CALCULATING SUPERSONIC BLUNT-BODY FLOW FIELDS WITH SHARP CORNERS AND EMBEDDED SHOCK WAVES | | 5. Report Date<br>November 1970 |
| | | 6. Performing Organization Code |
| 7. Author(s)<br>Richard W. Barnwell | | 8. Performing Organization Report No.<br>L-7284 |
| 9. Performing Organization Name and Address<br>NASA Langley Research Center<br>Hampton, Va. 23365 | | 10. Work Unit No.<br>129-01-22-10 |
| | | 11. Contract or Grant No. |
| 12. Sponsoring Agency Name and Address<br>National Aeronautics and Space Administration<br>Washington, D.C. 20546 | | 13. Type of Report and Period Covered<br>Technical Note |
| | | 14. Sponsoring Agency Code |
| 15. Supplementary Notes | | |

16. Abstract

A time-dependent numerical method for calculating supersonic blunt-body flow fields with sharp corners and embedded shock waves is presented. Axisymmetric and symmetric plane bodies can be treated. The method of characteristics is used at the bow shock wave and body surface, and a two-step finite-difference method of second-order accuracy is used between the shock and body. A stability analysis of the finite-difference equations which accounts for the effects of a nonorthogonal coordinate system is presented.

Calculations for flow over bodies with sharp and rounded corners are compared with experimental and other theoretical results. The influence of a parabolic free-stream velocity distribution on the flow over a spherically blunted cone is investigated, and a study of the effect of Mach number on the flow about a truncated cone is made.

| | | | |
|---|---|---|---|
| 17. Key Words (Suggested by Author(s))<br>Blunt-body flow fields<br>Sonic corners<br>Embedded shock waves<br>Time-dependent finite-difference method | 18. Distribution Statement<br>Unclassified – Unlimited | | |
| 19. Security Classif. (of this report)<br>Unclassified | 20. Security Classif. (of this page)<br>Unclassified | 21. No. of Pages<br>65 | 22. Price*<br>$3.00 |

*For sale by the Clearinghouse for Federal Scientific and Technical Information
Springfield, Virginia 22151

# A TIME-DEPENDENT METHOD FOR CALCULATING SUPERSONIC BLUNT-BODY FLOW FIELDS WITH SHARP CORNERS AND EMBEDDED SHOCK WAVES

By Richard W. Barnwell
Langley Research Center

## SUMMARY

A time-dependent numerical method for calculating supersonic blunt-body flow fields with sharp corners and embedded shock waves is presented. Axisymmetric and symmetric plane bodies can be treated. The method of characteristics is used at the bow shock wave and body surface, and a two-step finite-difference method of second-order accuracy is used between the shock and body. A stability analysis of the finite-difference equations which accounts for the effects of a nonorthogonal coordinate system is presented.

Calculations for flow over bodies with sharp and rounded corners are compared with experimental and other theoretical results. The influence of a parabolic free-stream velocity distribution on the flow over a spherically blunted cone is investigated, and a study of the effect of Mach number on the flow about a truncated cone is made.

## INTRODUCTION

Time-dependent methods provide a means of calculating supersonic flow past blunt bodies with forward-marching numerical techniques because the problem of transient flow has hyperbolic equations and is well posed as an initial-boundary-value problem. Results for steady flow are obtained from the asymptotic solution to the transient problem. These methods can be used to calculate blunt-body flow fields with complicating features such as sharp corners on the body contour, embedded shock waves, and large transonic regions.

A number of time-dependent methods have been developed for calculating flow past blunt bodies traveling at supersonic speeds. Evans and Harlow (ref. 1) introduced the particle-in-cell method, a finite-difference method of first-order accuracy in the mesh spacings which treats the bow shock wave as a continuous compression and which is formulated in a mixed Eulerian-Lagrangian frame of reference. Eulerian methods of first-order accuracy which treat the bow shock wave as a continuous compression have been developed by Rich and Blackman (ref. 2); Bohachevsky and Rubin (ref. 3); Gentry, Martin, and Daly (ref. 4); Barnwell (ref. 5); Rusanov (ref. 6); and others.

A finite-difference technique of second-order accuracy which treats shock waves as continuous compressions has been developed by Lax and Wendroff (ref. 7). This technique has been used by Burstein (ref. 8), Magnus and Gallaher (ref. 9), and others to solve the blunt-body problem.

Another approach to the blunt-body problem is to treat the bow shock wave as a discontinuity. Sauerwein (ref. 10) used this approach and calculated the flow field by using the time-dependent method of characteristics. Godunov, Prokopov, and Zabrodin (ref. 11) developed a finite-difference method of first-order accuracy which treats the bow shock wave as a discontinuity. This method has been extended and used to calculate complicated flow fields by Masson, Taylor, and Foster (ref. 12) and McNamara (ref. 13). Other methods which treat the bow shock wave as a discontinuity have been developed by Rusanov (ref. 14), Xerikos and Anderson (ref. 15), and Moretti and Abbett (ref. 16). The method of reference 16 employs the time-dependent method of characteristics at the bow shock and body surface, and a finite-difference technique of second-order accuracy between the shock and body.

The purpose of this paper is to extend the method of Moretti and Abbett (ref. 16) so that flow fields about bodies with sharp corners and flow fields containing embedded shock waves can be calculated. In order to facilitate calculations near sharp corners, a system of body-oriented coordinates which focuses at the corners is used, and a conserved form of the governing equations with derivatives which are well-behaved near the corners is employed. The use of the governing equations in conservation form also permits the calculation of flow fields containing embedded shock waves. An exact treatment is employed to determine the multiple-valued solution at the sharp corner. It should be noted that a brief description of the present method and some results calculated with it have been presented in reference 17.

## SYMBOLS

| | |
|---|---|
| $A_i,B_i,C_i,D_i$ | quantities defined by equations (5) |
| a | speed of sound, also radius of flat nose |
| B,C | matrices defined by equations (A2b) and (A2c) |
| D | vector defined by equation (A2d) |

| | |
|---|---|
| $E$ | matrix defined by equation (A12) |
| $e$ | eigenvalue of matrix $E$ |
| $\bar{e}$ | $\tilde{U}$, $\tilde{U} + a$, or $\tilde{U} - a$ |
| $F, F_c, F_R$ | quantities used in equation (B3) |
| $f$ | quantity defined by equation (8) |
| $G$ | matrix defined by equation (A8) |
| $g$ | quantity defined by equation (19), also eigenvalue of matrix $G$ |
| $H$ | total enthalpy, $\frac{\gamma}{\gamma - 1} \frac{p}{\rho} + \frac{1}{2}\left(u^2 + v^2\right)$ |
| $j$ | geometry index defined by equation (6) |
| $K_r$ | curvature of reference line |
| $K_s$ | curvature of shock |
| $L_x, L_y$ | wavelength of solutions in X- and Y-directions, respectively |
| $M$ | Mach number |
| $N$ | integer |
| $p$ | static pressure |
| $p_t$ | stagnation pressure |
| $R$ | distance from sharp corner |
| $R_b$ | radius of curvature of body contour segment |
| $r$ | perpendicular distance from axis of symmetry |
| $r_b$ | base radius |

|  |  |
|---|---|
| $r_c$ | radius of curvature of corner |
| $r_n$ | radius of curvature of nose |
| $r_1,r_2$ | quantities defined by equations (A6) |
| S | arc length of body contour segment |
| s | distance along surface from axis |
| $t,\tau$ | time |
| U,V | velocity components tangent to and normal to shock, respectively |
| $\tilde{U}$ | quantity defined by equation (A14) |
| u,v | velocity components normal to and tangent to body normals, respectively |
| $\bar{V}$ | magnitude of velocity |
| w | vector defined by equation (A2a) |
| $w_o$ | vector used in equation (A5) |
| x,X | distance along reference line from axis |
| Y | normalized distance from body surface defined by equation (9) |
| y | distance normal to reference line |
| $y_b$ | distance between reference line and body surface |
| z | distance along axis from stagnation point |
| $\alpha$ | exponent used in equation (B3), $0 \leqq \alpha$ |
| $\bar{\alpha}$ | complex exponent |
| $\beta$ | shock angle |

| | |
|---|---|
| $\gamma$ | ratio of specific heats |
| $\Delta t, \Delta \tau$ | mesh spacing for time |
| $\Delta X, \Delta Y$ | mesh spacings for X- and Y-coordinates |
| $\Delta \eta, \Delta \xi$ | mesh spacings for $\eta$- and $\xi$-coordinates |
| $\delta$ | thickness of shock layer |
| $\dot{\delta} = \frac{\partial \delta}{\partial t}$ or $\frac{\partial \delta}{\partial \tau}$ | |
| $\delta' = \frac{\partial \delta}{\partial x}$ or $\frac{\partial \delta}{\partial X}$ | |
| $\epsilon$ | percent deviation of free-stream velocity at distance $r = r_b$ from axis from center-line value |
| $\eta, \xi$ | coordinates along and normal to shock, respectively |
| $\bar{\eta}, \bar{\xi} = \frac{2\pi\ \Delta Y}{L_y}, \frac{2\pi\ \Delta X}{L_x}$ | |
| $\theta$ | angle between body normal and free-stream direction |
| $\kappa$ | damping coefficient which satisfies inequalities (15) |
| $\Lambda$ | quantity defined by equations (A6) |
| $\lambda_X$ | scale factor for X-coordinate |
| $\lambda_\eta$ | scale factor for $\eta$-coordinate |
| $\mu$ | quantity defined by equation (7) |
| $\rho$ | density |
| $\sigma$ | angle between normal to body surface and normal to shock wave |
| $\varphi$ | angle defined by equation (A13) |

| | |
|---|---|
| $\psi$ | angle defined by equation (A23) |

Subscripts:

| | |
|---|---|
| A,D | at base points of bicharacteristics |
| b | at body surface |
| C | at corner for $x = x_{c,min}$ |
| c | at corner |
| ℄ | on center line |
| $l$,m | indices for grid intersections for X- and Y-coordinates, respectively |
| max | maximum value |
| min | minimum value |
| s | immediately behind shock |
| $\infty$ | in free stream |

Superscripts:

| | |
|---|---|
| k | time index |
| * | denotes conditions for smallest value of $x$ where $u = a$ |
| $\tilde{()}$ | denotes first-order solution |

## ANALYSIS

The present method for calculating numerical solutions for time-dependent, inviscid, axisymmetric or symmetric plane flow past blunt bodies traveling at supersonic speeds is described in this section. The basic approach is the same as that of Moretti and Abbett (ref. 16) in that the method of characteristics is used at the bow shock wave and the body surface, and a second-order finite-difference method is used between the shock and surface. However, a different coordinate system is used in the present method, and a broader class of problems can be treated.

The problem of transient supersonic flow past blunt bodies is treated as an initial-boundary-value problem and is calculated with forward-marching techniques. From an initial solution which can be very approximate, the flow is calculated at successive time intervals in a closed region which is bounded by the bow shock wave, the body surface, the axis of symmetry, and a line extending from the body to the shock which is located downstream of the sonic line. At each time step, the flow is calculated first at points on the bow shock, then at points on the body, and finally, at points between the body and shock. Results for steady flow are obtained after many time steps when the time derivatives of the flow properties are sufficiently small.

## Calculations at Points Within the Shock Layer

The basic coordinate system which is used in this paper is curvilinear and is oriented with respect to the body as shown in figure 1. The coordinate $x$ is the distance along a reference line which is located a constant distance $y_b$ from the body surface, and the coordinate $y$ is the perpendicular distance to the reference line and is positive outward. The velocity components $u$ and $v$ which are used in this paper are normal to and tangent to the body normals, respectively, as shown in figure 1.

The geometry of the reference line is expressed in terms of its curvature $K_r$ and the angle $\theta$ between the normal to the reference line and a line parallel to the axis of symmetry. This angle is shown in figure 1. The quantities $K_r$ and $\theta$ are related by the equation

$$K_r = \frac{d\theta}{dx} \tag{1}$$

The quantity $r$ is the perpendicular distance from a point in the flow field to the axis of symmetry, and $\lambda_x$ is the scale factor for the x-coordinate. These quantities are given by the equations

$$r = \int_{\bar{x}=0}^{\bar{x}=x} \cos \theta(\bar{x})\, d\bar{x} + y \sin \theta(x) \tag{2}$$

and

$$\lambda_x = 1 + yK_r \tag{3}$$

The blunt bodies which are treated in this paper have profiles which are constructed of segments of constant curvature (straight-line segments and circular arcs). The curvature of a segment of the reference line is related to the distance $y_b$ and the radius of curvature $R_b$ of the corresponding body segment by the equation

$$K_r = \frac{1/R_b}{1 + \frac{y_b}{R_b}}$$

Straight body segments are associated with parallel straight reference line segments, whereas circular arcs on the body are associated with concentric circular arcs on the reference line. In the vicinity of a sharp corner, the reference line is a circular arc with the radius $y_b$. This arc extends from $x_{c,min}$, the value of $x$ on the perpendicular to the upstream surface at the corner, to $x_{c,max}$, the value of $x$ on the perpendicular to the downstream surface. The length of each segment of the reference line must be some integral multiple $N$ of the mesh spacing $\Delta x$. The magnitude of $\Delta x$ is related to the number $N$, the radius of curvature of the body segment $R_b$, and the arc length of the body segment $S$ by the equation

$$\Delta x = \frac{S}{N} \frac{R_b + y_b}{R_b}$$

If the cross section of the body is circular, the reference line can be constructed with a single segment, and the quantities $N$, $S$, $R_b$, and $y_b$ can be chosen independently. For bodies with two segments with different values of $S$ and $R_b$, the numbers $N_1$ and $N_2$ of mesh spacings $\Delta x$ which compose the respective reference line segments can be chosen independently, but both sets of quantities $S$, $R_b$, and $N$ must satisfy the equation for $\Delta x$. This condition is met if the distance $y_b$ satisfies the equation

$$\frac{S_1}{N_1} \frac{R_{b,1} + y_b}{R_{b,1}} = \frac{S_2}{N_2} \frac{R_{b,2} + y_b}{R_{b,2}}$$

When the body is constructed of three or more segments, the choice of $N$, $S$, and $R_b$ for each segment is not arbitrary.

The governing partial differential equations for inviscid axisymmetric and two-dimensional flow can be written in divergence form in terms of the coordinates $x$ and $y$ and the time $t$ as

$$\frac{\partial A_i}{\partial t} + \frac{\partial B_i}{\partial x} + \frac{\partial C_i}{\partial y} + D_i = 0 \qquad (i = 1,2,3,4) \qquad (4)$$

In equation (4), the subscript 1 denotes the continuity equation, the subscripts 2 and 3 denote the tangential and normal momentum equations, respectively, and the subscript 4 denotes the energy equation. The quantities $A_i$, $B_i$, $C_i$, and $D_i$ are written as follows:

$$\left.\begin{aligned}
A_1 &= \rho\lambda_x \\
A_2 &= \rho u\lambda_x \\
A_3 &= \rho v\lambda_x \\
A_4 &= (\rho H - p)\lambda_x \\
B_1 &= (1 + \mu j)\rho u \\
B_2 &= p + (1 + \mu j)\rho u^2 \\
B_3 &= (1 + \mu j)\rho uv \\
B_4 &= (1 + \mu j)\rho uH \\
C_1 &= \rho v\lambda_x \\
C_2 &= \rho uv\lambda_x \\
C_3 &= \left(p + \rho u^2\right)\lambda_x \\
C_4 &= \rho vH\lambda_x \\
D_1 &= j(1 - \mu)\rho u\lambda_x \cos\frac{\theta}{r} + j\rho vf \\
D_2 &= j(1 - \mu)\rho u^2\lambda_x \cos\frac{\theta}{r} + \rho uv\left(K_r + jf\right) \\
D_3 &= j(1 - \mu)\rho uv\lambda_x \cos\frac{\theta}{r} + j\rho v^2 f - \left(p + \rho u^2\right)K_r \\
D_4 &= j(1 - \mu)\rho uH\lambda_x \cos\frac{\theta}{r} + j\rho vHf
\end{aligned}\right\} \qquad (5)$$

where p, $\rho$, $\gamma$, and H are the pressure, density, ratio of specific heats, and total enthalpy, respectively. The quantities j, $\mu$, and f depend on the geometry and are given by the equations

$$j = \left\{ \begin{matrix} 0 & \text{(Two-dimensional flow)} \\ 1 & \text{(Axisymmetric flow)} \end{matrix} \right\} \tag{6}$$

$$\mu = \left\{ \begin{matrix} 1 & \text{(On the axis)} \\ 0 & \text{(Off the axis)} \end{matrix} \right\} \tag{7}$$

and

$$f = \left\{ \begin{matrix} K_r & \text{(On the axis)} \\ \dfrac{\lambda_x \sin \theta}{r} & \text{(Off the axis)} \end{matrix} \right\} \tag{8}$$

In order to prevent the bow shock from cutting across the grid lines, the y-coordinate is normalized with the local shock layer thickness $\delta$ as shown in figure 2. The normalized coordinate Y, which is given by the equation

$$Y = \frac{y + y_b}{\delta} \tag{9}$$

has the values of zero at the body surface and 1 at the shock wave. The partial derivatives with respect to the old independent variables t, x, and y are related to the partial derivatives with respect to the new variables $\tau = t$, $X = x$, and $Y = y$ by the expressions:

$$\frac{\partial}{\partial t} = \frac{\partial}{\partial \tau} - \frac{Y\dot{\delta}}{\delta} \frac{\partial}{\partial Y}$$

$$\frac{\partial}{\partial x} = \frac{\partial}{\partial X} - \frac{Y\delta'}{\delta} \frac{\partial}{\partial Y}$$

$$\frac{\partial}{\partial y} = \frac{1}{\delta} \frac{\partial}{\partial Y}$$

where $\dot{\delta}$ and $\delta'$ are the derivatives of $\delta$ with respect to $\tau$ and X, respectively. Equation (4) can be written in terms of $\tau$, X, and Y as

$$\frac{\partial A_i}{\partial \tau} = -\left\{\frac{\partial B_i}{\partial X} + \frac{1}{\delta}\frac{\partial}{\partial Y}\left[C_i - Y\left(A_i\dot{\delta} + B_i\delta'\right)\right] + D_i + \frac{1}{\delta}\left(A_i\dot{\delta} + B_i\delta'\right)\right\} \qquad (i = 1,2,3,4) \qquad (10)$$

There are several advantages to using the governing equations in this particular conservation form. In the first place, it improves the results at grid points adjacent to sharp corners because the quantities $C_i - Y\left(A_i\dot{\delta} + B_i\delta'\right)$ are proportional to $Y$ so that the derivatives of these quantities with respect to $Y$ in equation (10) are well-behaved at these points although the individual properties have large Y-derivatives there. This condition is true because the reference line subtending the corner is a circular arc with the curvature $K_r = \frac{1}{y_b}$ so that the scale factor $\lambda_x$ satisfies the equation

$$\lambda_x = \frac{\delta}{y_b} Y$$

and the following relationship holds:

$$C_i - y\left(A_i\dot{\delta} + B_i\delta'\right) \propto Y$$

In the second place, the conservation form permits the calculation of flow fields containing embedded shock waves, no special consideration being given to computations in the vicinity of those waves.

A two-step Lax-Wendroff finite-difference method is used to obtain solutions of second-order accuracy at points between the shock wave and body surface. The first step of the calculation is the determination of a solution of first-order accuracy in the mesh spacing $\Delta\tau$, $\Delta x$, and $\Delta Y$ at the new time $\tau$ from the known solution at time $\tau - \Delta\tau$, whereas the second step is the correction of the solution at time $\tau$ to second-order accuracy. Let $k$, $l$, and $m$ be the indices for the time $\tau$ and the coordinates $X$ and $Y$, respectively. The first-order solution at time $\tau$ is obtained with the equations

$$\left(\tilde{A}_i\right)_{l,m}^{k} = \frac{1}{4}\left[\left(A_i\right)_{l,m+1}^{k-1} + \left(A_i\right)_{l,m-1}^{k-1} + \left(A_i\right)_{l+1,m}^{k-1} + \left(A_i\right)_{l-1,m}^{k-1}\right] + \Delta\tau\left(\frac{\partial A_i}{\partial \tau}\right)_{l,m}^{k-1} \qquad (i = 1,2,3,4) \qquad (11)$$

where values for the partial derivatives $\partial A_i/\partial\tau$ at the point $(k - 1, l, m)$ are determined by evaluating the right-hand side of equation (10) at this point. The partial derivatives with respect to X and Y in equations (10) are approximated with central difference formulas. Once the quantities $A_i$ are known, the flow properties $p$, $\rho$, $u$, and $v$ can be determined. It should be noted that the scale factor $\lambda_x$, and hence the shock layer thickness $\delta$ at time $\tau$, is needed in order to determine the density from the known value of $A_1$. It is for this reason that for each new time step, the solutions at points on the bow shock wave are determined before the solutions at points between the shock and body.

The second-order solution at time $\tau$ is obtained with the equations

$$\left(A_i\right)_{l,m}^{k} = \left(A_i\right)_{l,m}^{k-1} + \frac{1}{2}\Delta\tau\left[\left(\frac{\partial A_i}{\partial\tau}\right)_{l,m}^{k-1} + \left(\frac{\partial\tilde{A}_i}{\partial\tau}\right)_{l,m}^{k}\right]$$
$$-\kappa\left[(\Delta X)^4\left(\frac{\partial^4 A_i}{\partial X^4}\right)_{l,m}^{k-1} + (\Delta Y)^4\left(\frac{\partial^4 A_i}{\partial Y^4}\right)_{l,m}^{k-1}\right] \qquad (i = 1,2,3,4) \qquad (12)$$

where the values for the partial derivatives $\partial A_i/\partial\tau$ at the point $(k, l, m)$ are determined by evaluating the right-hand side of equation (10) at this point with the first-order solution just obtained. The terms of fourth order in equations (12) are not physical and are added to eliminate instabilities.

The von Neumann conditions provide a means of estimating the upper bound of the time step $\Delta\tau$ which can be used with a given set of finite-difference equations. It is shown in appendix A that, in terms of the velocity components $u$ and $v$ and the nonorthogonal coordinates X and Y used in this paper, this condition can be written as

$$\Delta\tau \leqq \frac{\dfrac{\left(\lambda_x\,\Delta X\right)(\delta\,\Delta Y)}{\sqrt{\left(\lambda_x\,\Delta X\right)^2 + (\delta\,\Delta Y)^2}} \Bigg/ \left[\sqrt{u^2 + (v - Y\dot{\delta})^2} + a\right]}{\sqrt{1 + \dfrac{(Y\delta'\,\Delta X)^2}{\left(\lambda_x\,\Delta X\right)^2 + (\delta\,\Delta Y)^2} + \sqrt{\left[1 + \dfrac{(Y\delta'\,\Delta X)^2}{\left(\lambda_x\,\Delta X\right)^2 + (\delta\,\Delta Y)^2}\right]^2 - \left[\dfrac{2\left(\lambda_x\,\Delta X\right)(\delta\,\Delta Y)}{\left(\lambda_x\,\Delta X\right)^2 + (\delta\,\Delta Y)^2}\right]^2}}} \qquad (13)$$

where $a$ is the local speed of sound. In practice, it has been found that this inequality can be replaced by a simpler expression of the form

$$\Delta\tau \leqq \frac{1}{\sqrt{\gamma + 1}\;\bar{V}_{\max,\infty}}\min\left(\lambda_x\,\Delta X,\ \delta\,\Delta Y\right) \qquad (14)$$

where $\bar{V}_{max,\infty} = \sqrt{2H_\infty}$ is the maximum speed in the free stream. It is also shown in appendix A that the damping coefficient $\kappa$ in equation (12) must satisfy the inequalities

$$0 < \kappa \leq \frac{1}{32} \tag{15}$$

## Calculations at Points on Bow Shock Wave

As in reference 16, a time-dependent method of characteristics is employed at the shock wave and body surface. The present method differs from that of reference 16 in that the characteristic compatibility relation is integrated along a bicharacteristic rather than along a quasi-one-dimensional characteristic. A general discussion of the time-dependent method of characteristics for two-dimensional flow can be found in reference 10.

An orthogonal curvilinear coordinate system $\eta, \xi$ is established at the shock wave as shown in figure 3, where $\eta$ and $\xi$ are the distances along and normal to the shock, respectively, at time $\tau$. The velocity components in the $\eta$- and $\xi$-directions are U and V, respectively. The angle $\sigma$ between the normals to the shock wave and the reference line satisfies the relation

$$\tan \sigma = \frac{\delta'}{\lambda_x} \tag{16}$$

The basic problem is to determine the solution for the flow properties and the shock speed at points on the shock at time $\tau$ from the known solution at $\tau - \Delta\tau$. The equations which are solved at points on the shock wave are the Rankine-Hugoniot relations and one characteristic compatibility relation. If the subscripts $\infty$ and s denote the quantities in the free stream and immediately behind the shock, respectively, the Rankine-Hugoniot relations can be written as

$$\left.\begin{aligned}
&\rho_s\left(V_s - \sec\sigma\,\dot{\delta}\right) = \rho_\infty\left(V_\infty - \sec\sigma\,\dot{\delta}\right)\\
&p_s + \rho_s\left(V_s - \sec\sigma\,\dot{\delta}\right)^2 = p_\infty + \rho_\infty\left(V_\infty - \sec\sigma\,\dot{\delta}\right)^2\\
&\frac{\gamma}{\gamma - 1}\frac{p_s}{\rho_s} + \frac{1}{2}\left(V_s - \sec\sigma\,\dot{\delta}\right)^2 = \frac{\gamma}{\gamma - 1}\frac{p_\infty}{\rho_\infty} + \frac{1}{2}\left(V_\infty - \sec\sigma\,\dot{\delta}\right)^2\\
&U_s = U_\infty
\end{aligned}\right\} \tag{17}$$

The characteristic compatibility relation is written as

$$\frac{dp}{d\tau} + \rho a \frac{dV}{d\tau} = -\frac{1}{\lambda_\eta}\left[(1 + \mu j)\rho a^2 \frac{\partial U}{\partial \eta} + j(1 - \mu)\rho a^2 U \frac{\lambda_\eta}{r} \cos \beta \right.$$
$$\left. + \rho a^2 V\left(K_s + jg\right) - K_s \rho a U^2\right] \tag{18}$$

where $d/d\tau$ is the substantial derivative, $j$ and $\mu$ are given by equations (6) and (7), respectively, and $g$ is given by the equation

$$g = \left\{\begin{array}{ll} K_s & \text{(On the axis)} \\ \lambda_\eta \sin \beta/r & \text{(Off the axis)} \end{array}\right\} \tag{19}$$

The quantities $\beta$, $K_s$, and $\lambda_\eta$ in equation (18) are the angle between the normal to the shock wave and the free-stream direction, the curvature of the shock, and the scale factor for the $\eta$-coordinate, respectively, and are given by the equations

$$\beta = \theta - \sigma$$

$$K_s = \frac{\partial \beta}{\partial \eta}$$

$$\lambda_\eta = 1 + K_s \xi$$

The compatibility relation (18) is integrated from a point between the shock and body at time $\tau - \Delta\tau$ to the point on the shock at time $\tau$ along the bicharacteristic which satisfies the differential equations

$$\left.\begin{array}{l} \dfrac{d\eta}{d\tau} = \dfrac{U}{\lambda_\eta} \\ \\ \dfrac{d\xi}{d\tau} = V + a \end{array}\right\} \tag{20}$$

The equation thus obtained gives a linear relationship between the pressure $p_s$ and the velocity component normal to the shock $V_s$. This equation and the Rankine-Hugoniot relations (17) are solved simultaneously to determine values for the flow properties $p_s$, $\rho_s$, $U_s$, and $V_s$ and the component of the shock velocity normal to the reference line $\dot{\delta}$ at time $\tau$.

The following procedure is used to obtain solutions at the bow shock. First, a tentative value for $\delta(\eta,\tau)$, the location of the shock wave at time $\tau$, is obtained from the equation

$$\delta(\eta,\tau) = \delta(\eta,\tau - \Delta\tau) + \Delta\tau\,\dot{\delta}(\eta,\tau - \Delta\tau)$$

at all points on the shock wave, the derivative $\delta'(\eta,\tau)$ is determined geometrically, and the angle $\sigma$ is evaluated with equation (16). Then it is assumed that $\dot{\delta}(\eta,\tau) = \dot{\delta}(\eta,\tau - \Delta\tau)$, and an initial solution for $p_s$, $\rho_s$, $U_s$, and $V_s$ at time $\tau$ is obtained from equations (17).

The point A where the bicharacteristic through the shock point s intersects the plane $\tau - \Delta\tau$ is determined by iteration. In order to accomplish this iteration, equations (20) are approximated by the finite-difference expressions

$$\left.\begin{aligned} \frac{\Delta\eta}{\Delta\tau} &= \frac{1}{2}\left[\left(\frac{U}{\lambda_\eta}\right)_s + \left(\frac{U}{\lambda_\eta}\right)_A\right] \\ \frac{\Delta\xi}{\Delta\tau} &= \frac{1}{2}\left[(V + a)_s + (V + a)_A\right] \end{aligned}\right\} \qquad (21)$$

Initially, it is assumed that the properties at A have the same values as those at s. These values are substituted into equations (21) and a first estimate for the location of A is obtained. Improved values for $U_A$, $V_A$, and $a_A$ are determined by interpolating the known solution at time $\tau - \Delta\tau$ and are used in equations (21) to obtain a second estimate of the location of point A. This process is repeated until the results for the location of point A converge.

When point A has been located, the compatibility relation (18) is integrated from A to s along the bicharacteristic. In order to perform this integration, the right-hand side of equation (18) and the coefficient $\rho a$ on the left-hand side are evaluated at s and A, and the results are averaged. The integrated compatibility equation and the Rankine-Hugoniot relations (17) are solved simultaneously for improved values of the quantities $p_s$, $\rho_s$, $U_s$, $V_s$, and $\dot{\delta}$ at time $\tau$, and a second approximation for the shock location is determined with the equation

$$\delta(\eta,\tau) = \delta(\eta,\tau - \Delta\tau) + \frac{1}{2}\Delta\tau\left[\dot{\delta}(\eta,\tau - \Delta\tau) + \dot{\delta}(\eta,\tau)\right]$$

Once the improved solution has been obtained at all points on the shock wave, new estimates of the derivative $\delta'(\eta,\tau)$ and the shock angle $\sigma$ are determined for each point.

In general, the second set of values for the flow properties and shock velocity and location at time $\tau$ differ slightly from the first set. Converged results are obtained by repeating the process described several times, beginning with the location of the point A, and continuing until the next set of improved values for the flow properties and shock wave parameters have been determined.

## Calculations at Points on the Body Surface

The basic x,y coordinate system shown in figure 1 is used in connection with the time t at points on the body surface. Therefore, the governing partial differential equations are given by equations (4). These equations are combined linearly to obtain characteristic compatibility relations which are used in conjunction with the boundary condition

$$v = 0$$

to obtain solutions for the flow properties at the body surface. The pressure can be determined with the relation

$$\frac{dp}{dt} - \rho a \frac{dv}{dt} = -\frac{1}{\lambda_x}\left[(1 + \mu j)\rho a^2 \frac{\partial u}{\partial x} + j(1 - \mu)\rho a^2 u \frac{\lambda_x}{r} \cos\theta + \rho a^2 v\left(K_r + jf\right) - K_r \rho a u^2\right] \tag{22}$$

where j, $\mu$, and f are given by equations (6), (7), and (8), respectively. Equation (22) is integrated along the bicharacteristic which satisfies the differential relations

$$\left.\begin{aligned} \frac{dx}{dt} &= \frac{u}{\lambda_x} \\ \frac{dy}{dt} &= v - a \end{aligned}\right\} \tag{23}$$

The density is determined with the compatibility solution

$$\frac{dp}{dt} - a^2 \frac{d\rho}{dt} = 0 \tag{24}$$

which is integrated along the streamline which wets the body surface. This streamline has the slope

$$\frac{dx}{dt} = \frac{u}{\lambda_x} \tag{25}$$

in the x,t surface. The surface velocity is determined either from the transient Bernoulli equation

$$\frac{dH}{dt} - \frac{1}{\rho}\frac{\partial p}{\partial t} = 0 \tag{26}$$

which is integrated along the surface streamline or by the compatibility relation

$$\frac{dp}{dt} + \rho a \frac{du}{dt} = -\rho a^2\left(\frac{\partial v}{\partial y} + ju\,\frac{\cos\,\theta}{r}\right) \tag{27}$$

which is integrated along the bicharacteristic in the x,t surface with the slope

$$\frac{dx}{dt} = \frac{u + a}{\lambda_x} \tag{28}$$

An iterative procedure is used to determine the solution at the body surface at time t which is similar to that employed at the shock wave. For each cycle of the iteration, values for the flow properties are determined at all the points on the body surface. The iteration is continued until the solutions for successive cycles of the iteration converge. In order to start the first cycle, the values of the flow properties at time t are set equal to the known values at time $t - \Delta t$.

The basic procedure which is employed at the body surface consists of using equations (22), (24), and (26) or (27) to determine the pressure p, the density $\rho$, and the tangential velocity component u, respectively. This procedure is used to determine the solution for all values of x for which the surface is continuous and for $x = x_{c,min}$ if the flow approaching the corner is supersonic.

The location of point A, where the bicharacteristic through the body point b at time t satisfies the differential relationships (23) and intersects the surface $t - \Delta t$, is determined iteratively in the same manner that was used at the shock wave. The compatibility relation (22) is integrated from A to b to determine the pressure $p_b$. Then the intersection point B of the surface $t - \Delta t$ and the streamline bicharacteristic through b, which satisfies equation (25), is determined and equation (24) is integrated from B to b to obtain the density $\rho_b$. At this stage either equation (26) or equation (27) is integrated to determine the tangential velocity $u_b$. It should be noted that at the axis of symmetry, the condition $u_b = 0$ is imposed. When the transient Bernoulli equation (26) is used, the partial derivative $\partial p/\partial t$ is evaluated explicitly. If the x- and t-coordinates of the points D and b are denoted by $x_D$, $t - \Delta t$, and $x_b$, t, respectively, the finite-difference expression for this derivative is written as

$$\frac{\partial p}{\partial t} = \frac{1}{2}\left[\frac{p(x_b,t) - p(x_b,t - \Delta t)}{\Delta t} + \frac{p(x_D,t) - p(x_D,t - \Delta t)}{\Delta t}\right]$$

The density $\rho$ in equation (26) is approximated with the average of the densities at the points D and b.

If the flow approaching a sharp corner on the body contour is subsonic, an alternate procedure is used to determine the solution at the corner for $x = x_{c,min}$. This procedure consists of simultaneously solving the integrated energy equation (24) and either the integrated transient Bernoulli equation (26) or the integrated compatibility equation (27) subject to the sonic condition $u = a$.

It is shown in appendix B that the solution at the corner for

$$x_{c,min} \leqq x \leqq x_{c,max}$$

is the transient analog to the Prandtl-Meyer solution, which is given by equations (B5) and (B6).

## Initial and Boundary Conditions

A complete initial solution can be constructed from a specified shock shape and surface pressure distribution, both of which can be very approximate. In this paper, the initial shock shape is a conic section, and the surface pressure distribution for smooth bodies is the Newtonian distribution. If the body has a sharp corner where the flow is sonic, an empirical distribution with a singularity at the corner is used. It is assumed that the initial shock velocity is zero so that the flow properties at the shock wave can be determined completely with the Rankine-Hugoniot relations and the approximate shock shape. The density and tangential velocity at the surface are determined with the approximate surface pressure and the principles of conservation of surface entropy and total enthalpy. The initial properties at points between the body and shock are obtained by interpolating linearly between the body and shock along normals to the body surface.

As discussed previously, the boundary conditions applied at the shock and body are the Rankine-Hugoniot relations for a moving shock and the flow-tangency condition, respectively. The boundary condition at the axis of symmetry is that the tangential velocity vanish there. The flow properties at the downstream boundary are determined by extrapolation. If this boundary is located in a region where the flow is supersonic, the errors incurred by the extrapolation do not propagate back upstream and hence do not influence the calculation appreciably.

## RESULTS AND DISCUSSION

All the results which are presented are for a perfect gas with a ratio of specific heats of 7/5 and for axisymmetric bodies at zero angle of attack. Unless otherwise specified, the free stream is uniform. When it is feasible, the pressure distributions are normalized with the quantity $\rho_\infty \bar{V}_\infty^2$ instead of the stagnation pressure so that the calculated value of the stagnation pressure can be presented. Solutions are presented in detail for several cases and are compared with experimental and other theoretical results in order to demonstrate the accuracy of the method. In addition, results are presented for flow fields with nonuniform distributions of the free-stream properties and flow fields with overexpansion and recompression regions.

### Sample Calculations

Results are presented for the flow fields about two flat-face cylinders, one with a rounded corner and the other with a sharp corner, and a blunted cone with a sharp corner. For each of the flat-face cylinders, detailed comparisons are made between experimental results and the result of two calculations with different mesh spacings. In the case of the blunted cone, comparisons are made between experimental results and the results of the present and other methods.

Flat-face cylinder with rounded corner.- The ratio of the radius of the corner to the base radius is 0.4, and the free-stream Mach number is 2.49. The shock-wave and sonic-line locations are shown in figure 4, the surface pressures and velocity distributions are given in figure 5, and flow property profiles along several normals to the body surface are presented in figure 6. The results for solution 1 of the present method depicted in figures 4, 5, and 6 were calculated with a grid with 21 mesh spacings in the X-direction and 6 in the Y-direction. The results for solution 2 were calculated with a grid with 14 and 4 mesh spacings, respectively, in the X- and Y-directions.

The experimental data for the shock-wave location shown in figure 4 were obtained coincident with the data presented in reference 18. The experimental data for the pressure and velocity were obtained from reference 18 and are depicted in figure 5 with a solid line as a function of the distance s along the surface from the axis. The normal to the surface designated as I in figure 6 is coincident with the stagnation streamline, the normal designated as II intersects the body on the shoulder and is inclined at an angle of $30^\circ$ to the free-stream direction, and the one designated as III intersects the body at the junction of the shoulder and the afterbody.

Flat-face cylinder with sharp corner.- The Mach number for this case is 2.81. The shock-wave and sonic-line shapes are shown in figure 7, the surface pressure and velocity distributions are given in figure 8, and the flow property profiles along the stagnation streamline and the lines normal to the upstream and downstream portions of the body surface at the sharp corner are presented in figure 9. The experimental data shown in figures 7 and 8 were obtained from results given in reference 19. In figure 9, the normal to the body along the stagnation streamline is designated as I; the normal to the upstream face at the corner, where $X = X_{c,min}$, is designated as II; and the normal to the downstream face at the corner, where $X = X_{c,max}$, is designated as III.

It is seen in figures 7, 8, and 9 that the numerical solutions differ slightly as a result of different mesh spacing sizes. For example, the numerical values for the pressure on the face near the corner are higher than the experimental values, whereas the values for the velocity on the face are generally lower than the experimental results. Both of these trends decrease as the size of the mesh spacings is decreased. However, it can be seen in figures 8 and 9 that the two solutions have the same singular character in the vicinity of the sharp corner. Note that at a sharp corner, the velocity component $v$ shown in figure 9(d) is zero only where $x = x_{c,min}$. (See appendix B.)

Blunted cone with sharp corner.- The half-angle of the cone shown in figure 10 is $60^{\circ}$, and the nose of the cone is spherically blunted and the ratio of nose radius to base radius is 0.25.

In figure 10(a), the shape of the bow shock wave, as predicted by the present method for a free-stream Mach number of 4.63, is compared with that predicted experimental data (ref. 20) and by the one-strip method of integral relations (ref. 21). It is seen that the results of the method of integral relations are in better agreement with experiment than the present results in the stagnation region. In the vicinity of the sharp corner, both methods tend to underestimate the thickness of the shock layer. The results for the surface pressure distribution are compared with experiment in figure 10(b). As noted in reference 21, the method of integral relations tends to underestimate the pressure on the conical part of the body. It is seen that the present results show good agreement with experiment in this region.

The results of the present method and the method of integral relations for the shock shape and surface pressure distribution for a free-stream Mach number of 10 are compared in figure 11. Also shown in the figure are the results of Masson, Taylor, and Foster (ref. 12) for a free-stream Mach number of 9. As has been mentioned previously, the results of reference 12 were calculated with the Godunov method, which is a time-dependent method of first-order accuracy. Because results for different Mach numbers are being compared in figure 11, the pressure distributions are normalized with the stagnation-point pressure. It is seen that the present method predicts that the shock-layer thickness is less than that predicted by the other two methods at all points along the body and that the surface pressure is greater than that predicted by the other methods.

The differences in the free-stream Mach numbers for the results shown in this figure do not account for the differences in the results since the Mach numbers are so large. In fact, the pressure predicted by the Godunov method on the conical part of the body for a free-stream Mach number of 9 is less than that predicted by the present method for a free-stream Mach number of either 4.63 or 10.

It is seen in figures 10(b) and 11(b) that the present results for the surface pressure are irregular just upstream of the corner. This irregularity decreases as the grid is refined and is probably related to the mesh-spacing size effect observed for the flat-face cylinder with the sharp corner.

### Calculations for Nonuniform Free Stream

The magnitude of the free-stream velocity is assumed to vary parabolically with the perpendicular distance from the axis so that flow fields about bodies in a nonuniform free stream such as that found in some wind tunnels or in the wake of a forebody can be investigated. The expression for the velocity is written in the form

$$\bar{V}_\infty(r) = \bar{V}_{\infty,\mathbb{C}}\left[1 - \epsilon\left(r/r_b\right)^2\right]$$

where $\bar{V}_{\infty,\mathbb{C}}$ is the magnitude of the free-stream velocity at the center line, $r_b$ is the base radius of the body, and $\epsilon$ is the percent deviation of the free-stream velocity at a distance $r = r_b$ from the axis from the value $\bar{V}_{\infty,\mathbb{C}}$. It is assumed that the free-stream pressure and total enthalpy are constant and that the flow in the free stream is parallel to the axis. This type of nonuniformity leads to a strong dependence of the dynamic pressure on the distance from the center line and becomes more pronounced as the center-line Mach number is increased.

The body which is treated is a spherically blunted cone with a sharp corner, a half-angle of $60^\circ$, and a nose radius to base radius ratio of 0.25. The Mach number at the center line is 10.

Bow shock wave and sonic line shapes.- The locations of the shock waves and the sonic lines resulting from three nonuniform free streams are compared with those for the uniform free stream in figure 12. It can be seen that the nonuniformity has a marked influence everywhere in the flow field. The general trend as $\epsilon$ is increased is for the shock wave to move closer to the body in the stagnation region and further from the body in the transonic and supersonic regions. The sonic point at the bow shock moves outward away from the axis as $\epsilon$ is increased. The results indicate that the sonic point on the surface is positioned at the corner for $\epsilon = 0, 0.005$, and 0.01, but that it is located upstream of the corner for $\epsilon = 0.03$. This displacement of the sonic point will be discussed subsequently.

Also shown in the figure are the results of the one-strip method of integral relations for $\epsilon = 0.01$. The results were calculated with a modified form of the method described in reference 21.

Surface pressure distribution.- In figure 13, the surface pressure, which is made nondimensional with $\rho_{\infty,℄}\bar{V}^2_{\infty,℄}$, is plotted as a function of the distance along the surface from the axis. It can be seen that for values of $\epsilon$ of 0.005, 0.01, and 0.03, the pressure near the corner $(s/r_b \approx 0.8)$ is reduced by about 10, 20, and 50 percent, respectively. It should be noted that these pressure reductions are accompanied by equally severe reductions in the free-stream Mach number. At a distance $r = r_b$ from the axis, for $\epsilon = 0.005$, the free-stream Mach number is reduced by 9 percent from 10 to 9.1; for $\epsilon = 0.01$, it is reduced by 16 percent to 8.4; and for $\epsilon = 0.03$, it is reduced by 34 percent to 6.6.

The results of the one-strip method of integral relations for $\epsilon = 0.01$ are also shown in the figure. The close agreement of the results of the present method and those of the method of integral relations is encouraging in the absence of experimental data on the subject.

The Newtonian pressure distributions are presented in figure 13 for $\epsilon = 0$, 0.01, and 0.03. The standard Newtonian equation was used, but the radial dependence of the quantity $\rho_\infty \bar{V}^2_\infty$ was included. The results of the present method for $\epsilon = 0$ and 0.01 differ considerably from the Newtonian results as expected since the flow is subsonic all along the face and is singular at the corner. The Newtonian results for $\epsilon = 0.03$ indicate that the sonic point is located on the conical portion of the body upstream of the corner at approximately the same location as the present results. The two sets of results are in close agreement in the supersonic region.

In general, there is a reluctance to accept solutions which indicate that the sonic point on the surface of a body in a symmetric inviscid flow field is located on a straight segment of the surface. In fact, Nikolskii and Taganov (ref. 22) have proved that for plane potential flow such a solution cannot exist and Shifrin (ref. 23) has extended the proof to cover symmetric, nonisentropic plane flow. However, it should be noted that this proof does not apply directly to axisymmetric flow.

It is possible that the truncation error of the present method is responsible for the displacement of the sonic point upstream of the corner for the case $\epsilon = 0.03$ since this error is viscous-like. However, it is also possible that the present results represent the inviscid flow correctly, and that the displacement occurs because the dynamic pressure at points off the axis for $\epsilon = 0.03$ becomes too small to support subsonic flow at the surface all the way to the corner.

## Calculations for Overexpansion-Recompression Flow Fields

The bodies about which flow is calculated in this section are truncated cones with rounded shoulders between the face and conical afterbody. The flow overexpands around this shoulder and recompresses because of the presence of the afterbody. The recompression starts as a continuous compression on the surface of the afterbody just downstream of the shoulder. Experiments (refs. 19 and 24) show that if the flow has expanded to the supersonic state, the Mach lines in the compression region may converge so that an embedded shock wave is formed between the surface of the afterbody and the bow shock wave.

Comparisons with experiment and another theoretical method.- The free-stream Mach number is 1.79, and the configuration about which the flow is calculated is body 2 of reference 23. The half-angle of the conical afterbody of this configuration is $30^{\circ}$, and the ratios $a/r_b$ and $r_c/r_b$ are 0.344 and 0.2, respectively. The results of the present method, the one-strip method of integral relations by Traugott (ref. 25), and the experimental data of Hastings, Persh, and Redman (ref. 24) for the shock wave and sonic line locations, and the surface pressure distribution are shown in figures 14 and 15. The pressure distribution in figure 15 is normalized with the stagnation value because an experimental value for the stagnation pressure is not given in reference 24.

The shadowgraph of this flow field indicates that there is a weak embedded shock wave in the recompression region over the afterbody. The present results for the distributions of pressure in this region along the lines $Y = \text{Constant}$ are shown in figure 16. The abscissa is the distance from the upstream edge of the conical afterbody. These results indicate that the flow is being compressed, but the relative magnitude of the pressure increase is small and decreases as the distance from the surface is increased. The points where the experimentally observed shock wave crosses the lines $Y = \text{Constant}$, which are plotted on the figure, are located where the pressure gradient is relatively large.

Effect of Mach number on shock-wave and sonic-line locations.- The influence of the free-stream Mach number on the structure of the shock layer about a $45^{\circ}$ truncated cone with rounded shoulders is shown in figure 17. The relative magnitudes of the radius of the flat face, the corner radius, the length of the conical surface, and the base radius are 1, 0.25, 2, and 1.664, respectively. The cone is followed by a cylindrical afterbody. Results are presented for Mach numbers of $\infty$, 2.8, 2.6, 2.4, and 2.0.

Also shown in the figure are results for the flat-face cylinder with the same value of the ratio $r_c/a$ as the truncated cone-cylinder. Comparisons of the results for the two bodies show the influence of the conical portion of the truncated cone-cylinder on the flow field.

For a free-stream Mach number of infinity, the sonic line and bow shock wave in the nose regions of the two bodies coincide. Thus, the flow field ahead of the first shoulder of the truncated cone-cylinder is not influenced by the presence of the conical portion of the body. The flow expands around the first shoulder and becomes supersonic. It then compresses on the conical part of the body and becomes subsonic. At the second shoulder, it again expands to the supersonic state. Qualitatively, the structure of the shock layer for a free-stream Mach number of 2.8 is essentially the same as that for $M_\infty = \infty$. However, when $M_\infty = 2.8$, the relative size of the subsonic region over the conical part of the body is much larger.

The regions of subsonic flow are connected for a Mach number of 2.6; thus, the flow in the stagnation region is influenced by the presence of the afterbody. However, this influence is so slight that the locations of the bow shock wave in the nose regions of the truncated cone and flat face cylinder are essentially the same. It should be noted that a bubble of supersonic flow remains at the first shoulder.

When the Mach number is 2.4, the zone of subsonic flow over the conical portion of the body enlarges so that it extends all the way to the bow shock wave. There are two isolated regions of supersonic flow at this Mach number: one at the bow shock wave above the first shoulder, and one on the first shoulder. The conical part of the body still has little influence on the flow in the stagnation region; thus, the shock-detachment distances for the truncated cone and the flat cylinder are the same.

For a Mach number of 2, the flow field upstream of the second shoulder is subsonic with the exception of the supersonic bubble at the first shoulder. It is seen that at this Mach number the entire subsonic region is affected noticeably by the presence of the conical surface.

It should be noted that for $\gamma = 1.4$, the weak shock solution for flow over a pointed $45^{\circ}$ cone with the shock attached at the apex predicts that the flow at all points in the shock layer is supersonic when the Mach number is infinity and 2.8, and subsonic when the Mach number is 2.6 and 2.4. No attached-shock solution exists for a $45^{\circ}$ cone when $\gamma = 1.4$ and $M_\infty = 2$.

The compression which occurs over the conical part of the truncated cone starts on a continuous compression at the first shoulder. At higher free-stream Mach numbers, the compression fan probably merges to become a weak embedded shock wave which intersects the bow shock wave. On the basis of the present results, it cannot be determined whether the embedded shock forms since the present method smears weak shocks so that they cannot be distinguished from continuous compressions. It is clear that the continuous compression extends all the way to the bow shock wave for $M_\infty = 2$ because the flow is subsonic throughout the recompression region.

Effect of Mach number on surface pressure distribution.- In figure 18, the surface pressure distributions, which have been nondimensionalized with the stagnation pressure, are plotted as a function of distance along the surface from the axis for the five values of $M_\infty$. The stagnation-point pressure $p_t$ rather than the quantity $\rho_\infty \bar{V}_\infty^2$ is used for normalization because it leads to a better overall correlation of the results. The sonic pressure level and the values of the surface pressure for a pointed 45° cone with the shock attached at the apex are shown also. As noted before, no attached-shock solution exists when $M_\infty = 2$.

It is seen that the results correlate very well in the stagnation region. On the first shoulder a Mach number effect appears which becomes very pronounced on the conical part of the body. This effect is monotonic, the higher nondimensional pressures corresponding to the lower Mach numbers. Note that the distribution for $M_\infty = 2$ appears to provide an upper bound for the other distributions on the rear part of the conical surface, and that the other distributions tend to approach the surface pressure value for the pointed 45° cone at the appropriate Mach number. Mach number effects are observed on the downstream part of the second shoulder but they are small.

## CONCLUDING REMARKS

A time-dependent numerical method is presented for calculating supersonic blunt-body flow fields with sharp corners and embedded shock waves. Both axisymmetric and symmetric plane bodies can be treated. The method of characteristics for transient flow was used at the bow shock wave and body surface, and a two-step finite-difference method of second-order accuracy which employs a shock and body-oriented coordinate system is used between the bow shock and body surface. Exact closed form expressions are used to determine the multiple-valued solutions at the sharp corners. A stability analysis of the finite-difference equations which accounts for the effect of the nonorthogonal coordinate system is presented.

Some results for bodies with both sharp and rounded corners were compared with experimental data and other theoretical results to establish the accuracy of the method.

The method was used to investigate the effect of a parabolic free-stream velocity distribution on the flow field about a 60° blunted cone with a sharp corner and a ratio of nose radius to base radius of 0.25. It was found that this nonuniformity tended to decrease the thickness of the shock layer adjacent to the blunted nose and increase the thickness adjacent to the conical surface. In addition, it was shown that increasing the nonuniformity caused a large decrease in the pressure on the conical part of the body.

A study of the effect of free-stream Mach number on the flow about a 45° truncated cone-cylinder with rounded corners was also made. It was found that for free-stream

Mach numbers between 2 and infinity, the flow overexpanded to the supersonic state on the corner between the face and the conical surface and then recompressed on the conical surface. For Mach numbers of 2.4 and higher, the pressure on the conical surface approached the value for similar flow over a pointed cone. It should be noted that similar flow does not exist for a pointed 45° cone for free-stream Mach numbers much below 2.4. It was found that the pressure distribution on the conical afterbody for $M_\infty = 2$, when normalized with the stagnation value, serves as an upper bound for the normalized distribution for the larger free-stream Mach numbers. For free-stream Mach numbers of 2.4 and above, the bow-shock-wave location in the stagnation region is not influenced appreciably by the presence of the conical part of the body.

Langley Research Center,
National Aeronautics and Space Administration,
Hampton, Va., September 9, 1970.

# APPENDIX A

## STABILITY ANALYSIS FOR FINITE-DIFFERENCE EQUATIONS

In this appendix, the von Neumann condition for the linearized form of the present difference equations is determined. This condition specifies an upper bound for the mesh spacing $\Delta\tau$ above which it may be expected that the magnitude of a given infinitesimal error will increase at successive time steps. In general, difference schemes which amplify small errors produce solutions which either diverge or contain large errors.

The basic procedure used in this paper to determine the von Neumann condition is given by Richtmyer (ref. 26). A technique employed by Van Leer (ref. 27) is used to account for the difference in the mesh spacing sizes for the X- and Y-coordinates. A nonphysical dissipation function of fourth order similar to that used by Richtmyer and Morton (ref. 28) is employed to avoid neutral stability at points where the components of velocity vanish or are sonic. This treatment accounts for the nonorthogonal nature of the X,Y coordinate system.

The differential equations (10) can be written in matrix form as

$$\frac{\partial w}{\partial \tau} + \frac{B}{\lambda_X}\frac{\partial w}{\partial X} + \frac{C}{\delta}\frac{\partial w}{\partial Y} + D = 0 \tag{A1}$$

where the vectors w and D and the matrices B and C are written as

$$w = \begin{Bmatrix} \rho \\ u \\ v \\ p \end{Bmatrix} \tag{A2a}$$

$$B = \begin{bmatrix} u & 0 & 0 & 0 \\ 0 & u & 0 & 1/\rho \\ 0 & 0 & u & 0 \\ 0 & \rho a^2 & 0 & u \end{bmatrix} \tag{A2b}$$

$$C = \begin{bmatrix} \left(v - Y\dot{\delta} - \frac{Y\delta' u}{\lambda_x}\right) & -\frac{Y\delta'}{\rho\lambda_x} & \rho & 0 \\ 0 & \left(v - Y\dot{\delta} - \frac{Y\delta' u}{\lambda_x}\right) & 0 & -\frac{Y\delta'}{\rho\lambda_x} \\ 0 & 0 & \left(v - Y\dot{\delta} - \frac{Y\delta' u}{\lambda_x}\right) & 1/\rho \\ 0 & -\frac{Y\delta'\rho a^2}{\lambda_x} & \rho a^2 & \left(v - Y\dot{\delta} - \frac{Y\delta' u}{\lambda_x}\right) \end{bmatrix} \tag{A2c}$$

$$D = \begin{Bmatrix} \frac{j\rho u \cos\theta}{r} + \rho v\left(\frac{K_r}{\lambda_x} + \frac{j \sin\theta}{r}\right) \\ \frac{uvK_r}{\lambda_x} \\ -\frac{u^2K_r}{\lambda_x} \\ \frac{j\rho a^2 u \cos\theta}{\lambda_x} + \rho a^2 v\left(\frac{K_r}{\lambda_x} + \frac{j \sin\theta}{r}\right) \end{Bmatrix} \tag{A2d}$$

The expanded forms of the finite-difference equations (11) and (12) are

$$\tilde{w}^k_{l,m} = \frac{1}{4}\left(w^{k-1}_{l+1,m} + w^{k-1}_{l-1,m} + w^{k-1}_{l,m+1} + w^{k-1}_{l,m-1}\right) - \frac{1}{2}\frac{\Delta\tau}{\lambda_x \Delta X} B\left(w^{k-1}_{l+1,m} - w^{k-1}_{l-1,m}\right)$$
$$- \frac{1}{2}\frac{\Delta\tau}{\delta\,\Delta Y} C\left(w^{k-1}_{l,m+1} - w^{k-1}_{l,m-1}\right) - \Delta\tau\, D \tag{A3}$$

and

$$
\begin{aligned}
w_{l,m}^{k} = w_{l,m}^{k-1} &- \frac{1}{4}\frac{\Delta\tau}{\lambda_x\,\Delta X}B\left(\tilde{w}_{l+1,m}^{k} - \tilde{w}_{l-1,m}^{k} + w_{l+1,m}^{k-1} - w_{l-1,m}^{k-1}\right) \\
&- \frac{1}{4}\frac{\Delta\tau}{\delta\,\Delta Y}C\left(\tilde{w}_{l,m+1}^{k} - \tilde{w}_{l,m-1}^{k} + w_{l,m+1}^{k-1} - w_{l,m-1}^{k-1}\right) - \Delta\tau\,D \\
&-\kappa\left[\left(w_{l+2,m}^{k-1} - 4w_{l+1,m}^{k-1} + 6w_{l,m}^{k-1} - 4w_{l-1,m}^{k-1} + w_{l-2,m}^{k-1}\right)\right. \\
&\left.+ \left(w_{l,m+2}^{k-1} -4w_{l,m+1}^{k-1} + 6w_{l,m}^{k-1} - 4w_{l,m-1}^{k-1} + w_{l,m-2}^{k-1}\right)\right]
\end{aligned}
\tag{A4}
$$

respectively. In this appendix it shall be assumed that the matrices B and C are evaluated at the point $(k - 1, l, m)$.

Let the small errors be represented by a series of terms of the form

$$
w = w_0 g^k \exp\left[i\left(l\bar{\xi} + m\bar{\eta}\right)\right]
\tag{A5}
$$

where

$$
g = \exp(\bar{\alpha}\,\Delta\tau)
$$

$$
\bar{\xi} = \frac{2\pi}{L_x}\Delta X
$$

$$
\bar{\eta} = \frac{2\pi}{L_y}\Delta Y
$$

The quantities $L_x$ and $L_y$ are the wavelengths of the error solutions in the X- and Y-directions, respectively, and define the quantities $\Lambda$, $r_1$, and $r_2$ as

$$
\left.
\begin{aligned}
\Lambda &= \frac{\Delta\tau\sqrt{\left(\lambda_x\,\Delta X\right)^2 + (\delta\,\Delta Y)^2}}{\left(\lambda_x\,\Delta X\right)(\delta\,\Delta Y)} \\
r_1 &= \frac{1}{\Lambda}\frac{\Delta\tau}{\lambda_x\,\Delta X} \\
r_2 &= \frac{1}{\Lambda}\frac{\Delta\tau}{\delta\,\Delta Y}
\end{aligned}
\right\}
\tag{A6}
$$

The solution at time $\tau$ in terms of that at $\tau - \Delta\tau$ for a small time step $\Delta\tau$ is obtained by substituting equation (A5) into equations (A3) and (A4) and taking the limit as $\Delta\tau$ approaches zero so that the quantities $\Delta\tau$ D in equations (A3) and (A4) vanish. This solution is written as

$$w(X,Y,\tau) = Gw(X,Y,\tau - \Delta\tau) \tag{A7}$$

where the matrix G is given by the equation

$$\begin{aligned} G = {} & \left\{1 - 4\kappa\left[(1 - \cos\bar{\xi})^2 + (1 - \cos\bar{\eta})^2\right]\right\}I \\ & - \frac{1}{2}\Lambda^2\left(r_1B\sin\bar{\xi} + r_2C\sin\bar{\eta}\right)^2 \\ & - i\,\frac{1}{4}(2 + \cos\bar{\xi} + \cos\bar{\eta})\,\Lambda\left(r_1B\sin\bar{\xi} + r_2C\sin\bar{\eta}\right) \end{aligned} \tag{A8}$$

Equation (A8) is the amplification matrix for the difference scheme given by equations (A3) and (A4).

The solutions at times $\tau$ and $\tau - \Delta\tau$ are related also by the equation

$$w(X,Y,\tau) = e^{\bar{\alpha}\,\Delta\tau}w(X,Y,\tau - \Delta\tau) = gw(X,Y,\tau - \Delta\tau) \tag{A9}$$

It can be seen from equation (A9) that the magnitude of the solution at time $\tau$ is less than that at time $\tau - \Delta\tau$; hence, the solution satisfies the von Neumann condition for stability if the magnitude of g is less than one.

It can be shown by combining equations (A7) and (A9) that g represents the eigenvalues of the matrix G:

$$(G - Ig)w = 0 \tag{A10}$$

The quantity I is the identity matrix. An expression for g can be obtained from the secular equation for equation (A10):

$$\left|G - Ig\right| = 0 \tag{A11}$$

Let the matrix E and the quantities $\cos\varphi$ and $\tilde{U}$ be defined as

$$E = r_1B\sin\bar{\xi} + r_2C\sin\bar{\eta} \tag{A12}$$

$$\cos\varphi = \frac{r_1 \sin\bar{\xi} - r_2 \sin\bar{\eta}\left(Y\delta'/\lambda_x\right)}{\sqrt{\left[r_1 \sin\bar{\xi} - r_2 \sin\bar{\eta}\left(Y\delta'/\lambda_x\right)\right]^2 + r_2^2 \sin^2\bar{\eta}}} \tag{A13}$$

and

$$\tilde{U} = u \cos\varphi + (v - Y\dot{\delta})\sin\varphi \tag{A14}$$

Therefore, the matrix E can be written as

$$E = \sqrt{\left[r_1 \sin\bar{\xi} - r_2 \sin\bar{\eta}\left(Y\delta'/\lambda_x\right)\right]^2 + r_2^2 \sin^2\bar{\eta}}\begin{bmatrix} \tilde{U} & \rho\cos\varphi & \rho\sin\varphi & 0 \\ 0 & \tilde{U} & 0 & \cos\varphi/\rho \\ 0 & 0 & \tilde{U} & \sin\varphi/\rho \\ 0 & \rho a^2 \cos\varphi & \rho a^2 \sin\varphi & \tilde{U} \end{bmatrix} \tag{A15}$$

The eigenvalues of this matrix are

$$e = \sqrt{\left[r_1 \sin\bar{\xi} - r_2 \sin\bar{\eta}\left(Y\delta'/\lambda_x\right)\right]^2 + r_2^2 \sin^2\bar{\eta}}\;\bar{e} \tag{A16}$$

where $\bar{e}$ represents one of the values $\tilde{U}$, $\tilde{U} + a$, or $\tilde{U} - a$. The value $\tilde{U}$ is doubly degenerate. Equations (A8), (A11), (A15), and (A16) can be combined to yield the following expression for the eigenvalues of the matrix G:

$$g = 1 - 4\kappa\left[(1 - \cos\bar{\xi})^2 + (1 - \cos\bar{\eta})^2\right] - \frac{1}{2}\Lambda^2 e^2 - i\,\frac{1}{4}(2 + \cos\bar{\xi} + \cos\bar{\eta})\Lambda e \tag{A17}$$

The magnitudes of the eigenvalues g are given by the equation

$$|g|^2 = \left(1 - \frac{1}{2}\Lambda^2 e^2\right)^2 + \frac{1}{16}(2 + \cos\bar{\xi} + \cos\bar{\eta})^2\,\Lambda^2 e^2$$

$$+ 4\kappa\left[(1 - \cos\bar{\xi})^2 + (1 - \cos\bar{\eta})^2\right]\left\{4\kappa\left[(1 - \cos\bar{\xi})^2 + (1 - \cos\bar{\eta})^2\right] - 2 + e^2\Lambda^2\right\} \tag{A18}$$

Equation (A18) can be used to determine the minimum upper bound for $\Delta\tau$ which satisfies the von Neumann condition for stability. In order that the damping terms (the terms which are proportional to the damping coefficient $\kappa$) will not increase the magnitude of $g$, it is necessary that $\kappa$ not be negative and that the following inequality holds:

$$4\kappa\left[(1 - \cos\bar{\xi})^2 + (1 - \cos\bar{\eta})^2\right] - 2 + e^2\Lambda^2 < 0$$

When this inequality is combined with the Courant-Friedrichs Lewy stability condition $\left(e^2\Lambda^2 \leqq 1\right)$, an upper bound of 1/32 is obtained for $\kappa$. If the damping coefficient $\kappa$ satisfies the inequalities

$$0 \leqq \kappa \leqq 1/32$$

equation (A17) can be replaced by the inequality

$$\begin{aligned} |g|^2 \leqq 1 &+ \frac{1}{4}\left[\frac{1}{4}(\cos\bar{\xi} + \cos\bar{\eta})^2 + (\cos\bar{\xi} + \cos\bar{\eta}) - 3\right]\Lambda^2 e^2 \\ &+ \frac{1}{4}\Lambda^4 e^4 + 4\kappa\left[(1 - \cos\bar{\xi})^2 + (1 - \cos\bar{\eta})^2\right]\left(\Lambda^2 e^2 - 1\right) \end{aligned} \tag{A19}$$

The inequalities

$$(\cos\bar{\xi} + \cos\bar{\eta})^2 \leqq 2\left(\cos^2\bar{\xi} + \cos^2\bar{\eta}\right)$$

$$\cos\bar{\xi} + \cos\bar{\eta} \leqq 2$$

$$\sin^2\bar{\xi} + \sin^2\bar{\eta} \leqq 2$$

can be used to establish an upper bound for the right-hand side of inequality (A19). The resulting inequality can be written as

$$|g|^2 \leqq 1 + \frac{1}{4}\left\{\Lambda^2 e^2 + 16\kappa\left[(1 - \cos\bar{\xi})^2 + (1 - \cos\bar{\eta})^2\right]\right\}\left[\Lambda^2 e^2 - \frac{1}{2}\left(\sin^2\bar{\xi} + \sin^2\bar{\eta}\right)\right] \tag{A20}$$

Since the quantity $\left\{\Lambda^2 e^2 + 16\kappa\left[(1 - \cos\bar{\xi})^2 + (1 - \cos\bar{\eta})^2\right]\right\}$ is positive definite, the magnitude of $g$ is less than one only when the following inequality is satisfied:

$$\Lambda^2 e^2 \leqq \frac{1}{2}\left(\sin^2\bar{\xi} + \sin^2\bar{\eta}\right) \tag{A21}$$

From equation (A16) it follows that

$$e^2 \leqq \left[\left(r_1|\sin \bar{\xi}| + \frac{r_2|\sin \bar{\eta}|Y|\delta'|}{\lambda_x}\right)^2 + r_2^2|\sin \bar{\eta}|^2\right]\bar{e}_{max}^2 \tag{A22}$$

where

$$\bar{e}_{max} = |\tilde{U}| + a$$

The quantity $\cos \psi$ is defined so that

$$\cos \psi = \frac{|\sin \bar{\xi}|}{\sqrt{\sin^2\bar{\xi} + \sin^2\bar{\eta}}} \tag{A23}$$

The inequalities (A21) and (A22) and equation (A23) can be combined to yield the inequality

$$\begin{aligned}\frac{2\Lambda^2 e^2}{\sin^2\bar{\xi} + \sin^2\bar{\eta}} &\leqq 2\Lambda^2\left[\left(r_1 \cos \psi + \frac{r_2 \sin \psi\ Y|\delta'|}{\lambda_x}\right)^2 + r_2^2 \sin^2\psi\right]\bar{e}_{max}^2 \\ &\leqq \Lambda^2\left\{1 + \left(Y\delta'/\lambda_x\right)^2 + \sqrt{\left[1 + \left(Y\delta'/\lambda_x\right)^2\right]^2 - 4r_1^2r_2^2}\right\}\bar{e}_{max}^2 \leqq 1\end{aligned} \tag{A24}$$

With this inequality and the definitions of $\Lambda$, $r_1$, $r_2$, and $\tilde{U}$ given in equations (A6) and (A14), it can be shown that $\Delta\tau$ must satisfy the following condition if the von Neumann stability criterion is to be observed:

$$\Delta\tau \leqq \frac{\dfrac{\left(\lambda_x\,\Delta X\right)(\delta\,\Delta Y)}{\sqrt{\left(\lambda_x\,\Delta X\right)^2 + (\delta\,\Delta Y)^2}}\Bigg/\left[\sqrt{u^2 + (v - Y\dot{\delta})^2} + a\right]}{\sqrt{1 + \dfrac{(Y\delta'\,\Delta X)^2}{\left(\lambda_x\,\Delta X\right)^2 + (\delta\,\Delta Y)^2} + \sqrt{\left[1 + \dfrac{(Y\delta'\,\Delta X)^2}{\left(\lambda_x\,\Delta X\right)^2 + (\delta\,\Delta Y)^2}\right]^2 - \left[\dfrac{2\left(\lambda_x\,\Delta X\right)(\delta\,\Delta Y)}{\left(\lambda_x\,\Delta X\right)^2 + (\delta\,\Delta Y)^2}\right]^2}}} \tag{A25}$$

The smallest value of the right-hand side of this inequality which occurs anywhere in the flow field at a given time step constitutes the least upper bound for $\Delta\tau$ for that particular time step. It can be seen that the magnitude of the right-hand side of inequality (A25) diminishes when the shock slope $\delta'$ becomes large (in other words, when the $X,Y$ coordinate system becomes skewed). However, there is a compensating effect since the scale factor $\lambda_x$ and the shock-layer thickness $\delta$ are generally large in regions where the coordinate system is skewed.

For the calculations which are presented in this paper, it has been found that the least upper bound is located generally in regions where the scale factor $\lambda_x$ or the shock-layer thickness $\delta$ are small rather than in regions where the shock slope $\delta'$ is large. Since only convex bodies are treated in this paper, the smallest value of $\lambda_x$ occurs on the body surface at the segment with the smallest radius of curvature. In the case of bodies with sharp corners, the smallest pertinent value of $\lambda_x$ occurs on the line $Y = \Delta Y$ where it subtends the corner. In general, the shock-layer thickness $\delta$ either attains or approaches its smallest value at the axis of symmetry. Therefore, the mesh spacings $\lambda_x \, \Delta X$ and $\delta \, \Delta Y$ either approach or attain their smallest values on or near the stagnation streamline.

The right-hand side of inequality (A25) can be simplified considerably when it is applied on the stagnation streamline since $\delta' = 0$ on the axis of symmetry and $Y = 0$ on the body surface. The expression for the upper bound of $\Delta\tau$ which can be used on the stagnation streamline is

$$\Delta\tau \leqq \frac{\min\left(\lambda_x \, \Delta X, \delta \, \Delta Y\right)}{\sqrt{2}\left[\sqrt{u^2 + (v - Y\dot{\delta})^2} + a\right]} \tag{A26}$$

Since the shock speed is generally much smaller than the magnitude of the velocity, the term in inequality (A26) which is proportional to $\dot{\delta}$ can be neglected for practical purposes. Thus, the least upper bound for $\Delta\tau$ is determined from the smallest value of the mesh spacings $\lambda_x \, \Delta X$ and $\delta \, \Delta Y$ and the largest value of the sum $\bar{V} + a$, where $\bar{V}$ is the total magnitude of the velocity. By using Bernoulli's equation, this sum can be written as

$$\bar{V} + a = a + \sqrt{2\left(H - \frac{a^2}{\gamma - 1}\right)} \tag{A27}$$

It can be shown that the maximum value of $\bar{V} + a$ for a given value of the total enthalpy $H$ is

$$\left\{\bar{V} + a\right\}_{max} = \sqrt{(\gamma + 1)H} = \sqrt{\frac{\gamma + 1}{2}} \, \bar{V}_{max} \tag{A28}$$

Since the total enthalpy does not change much during the course of a time-dependent calculation, the value of $\bar{V}_{max}$ in the undisturbed free stream can be used safely in equation (A28). From the inequality (A26) and equation (A28), the following expression is obtained for the least upper bound of $\Delta\tau$:

$$\Delta\tau \leqq \frac{1}{\sqrt{\gamma + 1}\,\bar{V}_{max,\infty}} \min\left(\lambda_x \Delta X, \delta \Delta Y\right) \tag{A29}$$

The effect of the damping terms in equation (A17) is to prevent the finite-difference equations from becoming neutrally stable when one or more of the eigenvalues $e$ vanish. Neutral stability occurs when the eigenvalue $g$ has a magnitude of 1 $\left(|g| = 1\right)$. If the finite-difference equations are neutrally stable in terms of a linear analysis, it is quite possible that the nonlinear effects which have been neglected in the linear analysis will be sufficient to render the calculation unstable. It is seen from equations (A14) and (A16) that an eigenvalue $e$ can vanish whenever one of the components $u$ or $(v - Y\dot{\delta})$ vanishes or becomes sonic.

It can be seen from equation (A17) that maximum damping occurs for $L_x = 2\ \Delta X$ and $L_y = 2\ \Delta Y$ although solutions with wavelengths of two mesh spacings are not observable. It is also seen that the damping decreases monotonically as the wavelengths of the disturbances increase. Therefore, the effect of the damping terms is to decrease the amplitude of short waves and to have very little influence on long waves. This is the desired effect since the physical solution being sought is generally characterized by wavelengths much longer than the mesh spacings being used, and solutions with wavelengths of only a few mesh spacings are generally unwanted disturbances.

# APPENDIX B

## PRANDTL-MEYER SOLUTION FOR THE TRANSIENT FLOW AT A SHARP CORNER

In this appendix, the solution for compressible, time-dependent flow at a sharp corner is presented. It is shown that this solution is multiple valued and satisfies the Prandtl-Meyer equations. It should be emphasized that the solution is applicable only at the corner and is not valid in general in any neighborhood of the corner.

When a perfect gas is being treated, equations (4) can be written as

$$\left.\begin{aligned}
&\frac{\partial\rho}{\partial t}+\frac{u}{\lambda_x}\frac{\partial\rho}{\partial x}+v\frac{\partial\rho}{\partial y}+\frac{\rho}{\lambda_x}\frac{\partial u}{\partial x}+\rho\frac{\partial v}{\partial y}+j\rho u\frac{\cos\theta}{r}+\rho v\left(\frac{K_r}{\lambda_x}+j\frac{\sin\theta}{Y}\right)=0\\
&\frac{\partial u}{\partial t}+\frac{u}{\lambda_x}\frac{\partial u}{\partial x}+v\frac{\partial u}{\partial y}+\frac{1}{\rho\lambda_x}\frac{\partial p}{\partial x}+\frac{K_r}{\lambda_x}uv=0\\
&\frac{\partial v}{\partial t}+\frac{u}{\lambda_x}\frac{\partial v}{\partial x}+v\frac{\partial v}{\partial y}+\frac{1}{\rho}\frac{\partial p}{\partial y}-\frac{K_r}{\lambda_x}u^2=0\\
&\frac{\partial p}{\partial t}+\frac{u}{\lambda_x}\frac{\partial p}{\partial x}+v\frac{\partial p}{\partial y}-\frac{\gamma p}{\rho}\left(\frac{\partial\rho}{\partial t}+\frac{u}{\lambda_x}\frac{\partial\rho}{\partial x}+v\frac{\partial\rho}{\partial y}\right)=0
\end{aligned}\right\}\qquad\text{(B1)}$$

It should be noted that the curvature of that part of the reference line which subtends the corner is

$$K_r=\frac{1}{y_b}$$

Let $x_{c,max}$ and $x_{c,min}$ be the maximum and minimum values, respectively, of the coordinate $x$ associated with the corner. If the angle $\theta$ for $x_{c,min}$ is denoted by $\theta_c$, then the function $\theta(x)$ can be written as

$$\theta=\theta_c+\frac{x-x_{c,min}}{y_b}$$

for $x_{c,min}\leqq x\leqq x_{c,max}$. Let a new independent variable $R$ be defined such that

$$R=y+y_b$$

This coordinate is measured from the corner along lines perpendicular to the reference surface. It should be noted that $\lambda_x$ and $r$ are written in terms of $R$ and $\theta$ as

$$\lambda_x = \frac{R}{y_b}$$

$$r = r_b + R \sin \theta$$

where $r_b$ is the perpendicular distance from the corner to the axis of symmetry. Equations (B1) are written in terms of $R$, $\theta$, and $t$ as

$$\left.\begin{aligned}
&\frac{\partial \rho}{\partial t} + \frac{u}{R}\frac{\partial \rho}{\partial \theta} + v\frac{\partial \rho}{\partial R} + \frac{\rho}{R}\frac{\partial u}{\partial \theta} + \rho\frac{\partial v}{\partial R} + j\rho u\frac{\cos\theta}{r_b + R\sin\theta} + \rho v\left(\frac{1}{R} + j\frac{\sin\theta}{r_b + R\sin\theta}\right) = 0 \\
&\frac{\partial u}{\partial t} + \frac{u}{R}\frac{\partial u}{\partial \theta} + v\frac{\partial u}{\partial R} + \frac{1}{\rho R}\frac{\partial p}{\partial \theta} + \frac{uv}{R} = 0 \\
&\frac{\partial v}{\partial t} + \frac{u}{R}\frac{\partial v}{\partial \theta} + v\frac{\partial v}{\partial R} + \frac{1}{\rho}\frac{\partial p}{\partial R} - \frac{u^2}{R} = 0 \\
&\frac{\partial p}{\partial t} + \frac{u}{R}\frac{\partial p}{\partial \theta} + v\frac{\partial p}{\partial R} - \frac{\gamma p}{\rho}\left(\frac{\partial \rho}{\partial t} + \frac{u}{R}\frac{\partial \rho}{\partial \theta} + v\frac{\partial \rho}{\partial R}\right) = 0
\end{aligned}\right\} \tag{B2}$$

Let the flow properties $p$, $\rho$, $u$, and $v$ in the vicinity of the corner be represented by functions of the form

$$F(t,R,\theta) = F_c(t,\theta) + R^{\alpha(t,\theta)}F_R(t,R,\theta) \tag{B3}$$

where $F_R(t,R,\theta)$ is bounded for small values of $R$ and the exponent is greater than or equal to zero. If these functions are substituted into equations (B2), and if these equations are then multiplied by $R$ and the limit is taken as $R$ approaches zero, the terms involving $\alpha$ and $F_R$ are eliminated and the following equations are obtained:

$$u_c\frac{\partial \rho_c}{\partial \theta} + \rho_c\frac{\partial u_c}{\partial \theta} + \rho_c V_c = 0 \tag{B4a}$$

$$\rho_c u_c\left(\frac{\partial u_c}{\partial \theta} + v_c\right) + \frac{\partial p_c}{\partial \theta} = 0 \tag{B4b}$$

$$\rho_c u_c\left(\frac{\partial v_c}{\partial \theta} - u_c\right) = 0 \tag{B4c}$$

$$\rho_c \frac{\partial p_c}{\partial \theta} - \gamma p_c \frac{\partial \rho_c}{\partial \theta} = 0 \tag{B4d}$$

These equations are the Prandtl-Meyer equations where, by assumption, $p_c$, $\rho_c$, $u_c$, and $v_c$ are functions of the time $t$ as well as of the angle $\theta$.

The solution for the flow properties $p$, $\rho$, $u$, and $v$ at the corner are of the form

$$F(t,x,y) = F_c(t,\theta)$$

where $x_{c,min} \leqq x \leqq x_{c,max}$ and $y = -y_b$. If $x^* \geqq x_{c,min}$ is the smallest value of $x$ associated with the corner for which $u = a$, if $\theta^*$ is the angle $\theta$ for $x = x^*$, and if the flow properties and the angle $\theta$ for $x = x_{c,min}$ are denoted by $p_C$, $\rho_C$, $u_C$, and $\theta_C$, respectively, then the solution at the corner which satisfies equations (B4) can be written as

$$\left.\begin{aligned} p &= p_C \\ \rho &= \rho_C \\ u &= u_C \cos\left(\theta - \theta_C\right) \\ v &= u_C \sin\left(\theta - \theta_C\right) \end{aligned}\right\} \tag{B5}$$

for $x_{c,min} \leqq x \leqq x^*$ and

$$p = p_C\left(\left\{\cos\left[\sqrt{\frac{\gamma - 1}{\gamma + 1}}(\theta - \theta^*)\right] - \sqrt{\frac{\gamma - 1}{\gamma + 1}\left(M_C^2 - 1\right)}\sin\left[\sqrt{\frac{\gamma - 1}{\gamma + 1}}(\theta - \theta^*)\right]\right\}\right)^{\frac{2\gamma}{\gamma-1}} \tag{B6a}$$

$$\rho = \rho_C\left(\left\{\cos\left[\sqrt{\frac{\gamma - 1}{\gamma + 1}}(\theta - \theta^*)\right] - \sqrt{\frac{\gamma - 1}{\gamma + 1}\left(M_C^2 - 1\right)}\sin\left[\sqrt{\frac{\gamma - 1}{\gamma + 1}}(\theta - \theta^*)\right]\right\}\right)^{\frac{2}{\gamma-1}} \tag{B6b}$$

$$u = a_C \left\{ \cos\left[\sqrt{\frac{\gamma - 1}{\gamma + 1}}(\theta - \theta^*)\right] - \sqrt{\frac{\gamma - 1}{\gamma + 1}\left(M_C^2 - 1\right)} \sin\left[\sqrt{\frac{\gamma - 1}{\gamma + 1}}(\theta - \theta^*)\right] \right\} \tag{B6c}$$

$$v = a_C \left\{ \sqrt{M_C^2 - 1} \cos\left[\sqrt{\frac{\gamma - 1}{\gamma + 1}}(\theta - \theta^*)\right] + \sqrt{\frac{\gamma + 1}{\gamma - 1}} \sin\left[\sqrt{\frac{\gamma - 1}{\gamma + 1}}(\theta - \theta^*)\right] \right\} \tag{B6d}$$

for $x_{c,max} \geqq x \geqq x^*$. The quantities $a_C$ and $M_C$ in equations (B6) are the speed of sound and the Mach number, respectively, at the corner for $x = x_{c,min}$.

# REFERENCES

1. Evans, Martha W.; and Harlow, Francis H.: The Particle-in-Cell Method for Hydrodynamic Calculations. LA-2139 (Contract W-7405-ENG. 36), Los Alamos Sci. Lab., Univ. of California, Nov. 8, 1957.
2. Rich, Marvin; and Blackman, Samuel: A Method for Eulerian Fluid Dynamics. LAM 2826 (Contract W-7405-ENG 36), Los Alamos Sci. Lab., Univ. of California, Mar. 29, 1963.
3. Bohachevsky, Ihor O.; and Rubin, Ephraim L.: A Direct Method for Computation of Nonequilibrium Flows With Detached Shock Waves. AIAA J., vol. 4, no. 4, Apr. 1966, pp. 600-607.
4. Gentry, Richard A.; Martin, Robert E.; and Daly, Bart J.: An Eulerian Differencing Method for Unsteady Compressible Flow Problems. J. Comput. Phys., vol. 1, no. 1, Aug. 1966, pp. 87-118.
5. Barnwell, Richard W.: Numerical Results for the Diffraction of a Normal Shock Wave by a Sphere and for the Subsequent Transient Flow. NASA TR R-268, 1967.
6. Rusanov, V. V. (D. A. Sinclair, trans.): Calculation of Interaction of Non-Steady Shock Waves With Obstacles. Tech. Transl. TT-1027, Nat. Res. Counc. Can. (Ottawa), 1962.
7. Lax, Peter D.; and Wendroff, Burton: Difference Schemes for Hyperbolic Equations With High Order of Accuracy. Commun. Pure Appl. Math., vol. XVII, no. 3, Aug. 1964, pp. 381-398.
8. Burstein, Samuel Z.: Finite-Difference Calculations for Hydrodynamic Flows Containing Discontinuities. J. Comput. Phys., vol. 1, no. 2, Nov. 1966, pp. 198-222.
9. Magnus, R. J.; and Gallaher, W. H.: Development of a Program for Calculating Viscous Supersonic Flow Over Blunted Cones. AFFDL-TR-68-28, U.S. Air Force, June 1968.
10. Sauerwein, Harry: A General Numerical Method of Characteristics. AIAA Pap. No. 65-25, Jan. 1965.
11. Godunov, S. K.; Prokopov, G. P.; and Zabrodin, A. V.: A Difference Scheme for Two-Dimensional Non-Steady Problems of Gas Dynamics and Calculation of Stream Flow With a Detached Shock Wave. UCRL-Trans-1060/L/, Lawrence Radiat. Lab., Univ. of California, Mar. 26, 1965.

12. Masson, B. S.; Taylor, T. D.; and Foster, R. M.: Application of Godunov's Method to Blunt-Body Calculations. AIAA J., vol. 7, no. 4, Apr. 1969, pp. 694-698.

13. McNamara, William: FLAME Computer Code for the Axisymmetric Interaction of a Blast Wave With a Shock Layer on a Blunt Body. J. Spacecraft Rockets, vol. 4, no. 6, June 1967, pp. 790-795.

14. Rusanov, V. V.: Three-Dimensional Flow About an Arbitrary Blunt Body. Aerospace Proceedings 1966, Vol. I, Joan Bradbrooke, Joan Bruce, and Robert R. Dexter, eds., Macmillan Co., 1966, pp. 291-301.

15. Xerikos, J.; and Anderson, W. A.: A Time-Dependent Approach to the Numerical Solution of the Flow Field About an Axisymmetric Vehicle at Angle of Attack. DAC-62279 (Contract NAS 8-21141), Douglas Aircraft Co., June 1968. (Available as NASA CR-61982.)

16. Moretti, Gino; and Abbett, Michael: A Time-Dependent Computational Method for Blunt Body Flows. AIAA J., vol. 4, no. 12, Dec. 1966, pp. 2136-2141.

17. Barnwell, Richard W.: Time-Dependent Numerical Method for Treating Complicated Blunt-Body Flow Fields. Analytical Methods in Aircraft Aerodynamics, NASA SP-228, 1970, pp. 177-195.

18. Stallings, Robert L., Jr.; and Howell, Dorothy T.: Experimental Pressure Distributions for a Family of Blunt Bodies at Mach Numbers From 2.49 to 4.63 and Angles of Attack From $0^{\circ}$ to $15^{\circ}$. NASA TN D-5392, 1969.

19. Kendall, James M., Jr.: Experiments on Supersonic Blunt-Body Flows. Progr. Rep. No. 20-372 (Contract No. DA-04-495-Ord 18), Jet Propulsion Lab., California Inst. Technol., Feb. 27, 1959.

20. Stallings, Robert L., Jr.; and Tudor, Dorothy H.: Experimental Pressure Distributions on a $120^{\circ}$ Cone at Mach Numbers From 2.96 to 4.63 and Angles of Attack From $0^{\circ}$ to $20^{\circ}$. NASA TN D-5054, 1969.

21. South, Jerry C., Jr.: Calculation of Axisymmetric Supersonic Flow Past Blunt Bodies With Sonic Corners, Including a Program Description and Listing. NASA TN D-4563, 1968.

22. Nikolskii, A. A.; and Taganov, G. I.: Gas Motion in a Local Supersonic Region and Conditions of Potential-Flow Breakdown. NACA TM 1213, 1949.

23. Shifrin, É. G.: The Direct Problem of Plane Symmetrical Flow With Detached Shock Wave About a Smooth Convex Profile. Sov. Phys. – Doklady, vol. 12, no. 1, July 1967, pp. 4-6.

24. Hastings, S. M.; Persh, J.; and Redman, E. J.: Experimental Investigation of the Pressure Distribution on Axi-Symmetric Flat-Face Cone-Type Bodies at Supersonic and Hypersonic Speeds. NAVORD Rep. 5659, U.S. Navy, Oct. 1, 1957.

25. Traugott, Stephen C.: An Approximate Solution of the Direct Supersonic Blunt-Body Problem for Arbitrary Axisymmetric Shapes. J. Aerosp. Sci., vol. 27, no. 5, May 1960, pp. 361-370.

26. Richtmyer, Robert D.: A Survey of Difference Methods for Non-Steady Fluid Dynamics. NCAR Tech. Notes 63-2, Nat. Center Atmos. Res., Aug. 27, 1962.

27. Van Leer, B.: Stabilization of Difference Schemes for the Equations of Inviscid Compressible Flow by Artificial Diffusion. J. Comput. Phys., vol. 3, no. 4, Apr. 1969, pp. 473-485.

28. Richtmyer, R. D.; and Morton, K. W.: Stability Studies With Difference Equations. (I) Non-Linear Stability. (II) Coupled Sound and Heat Flow. NYO-1480-5 (Contract AT(30-1)-1480) Courant Inst. Math. Sci., New York Univ., Aug. 25, 1964.

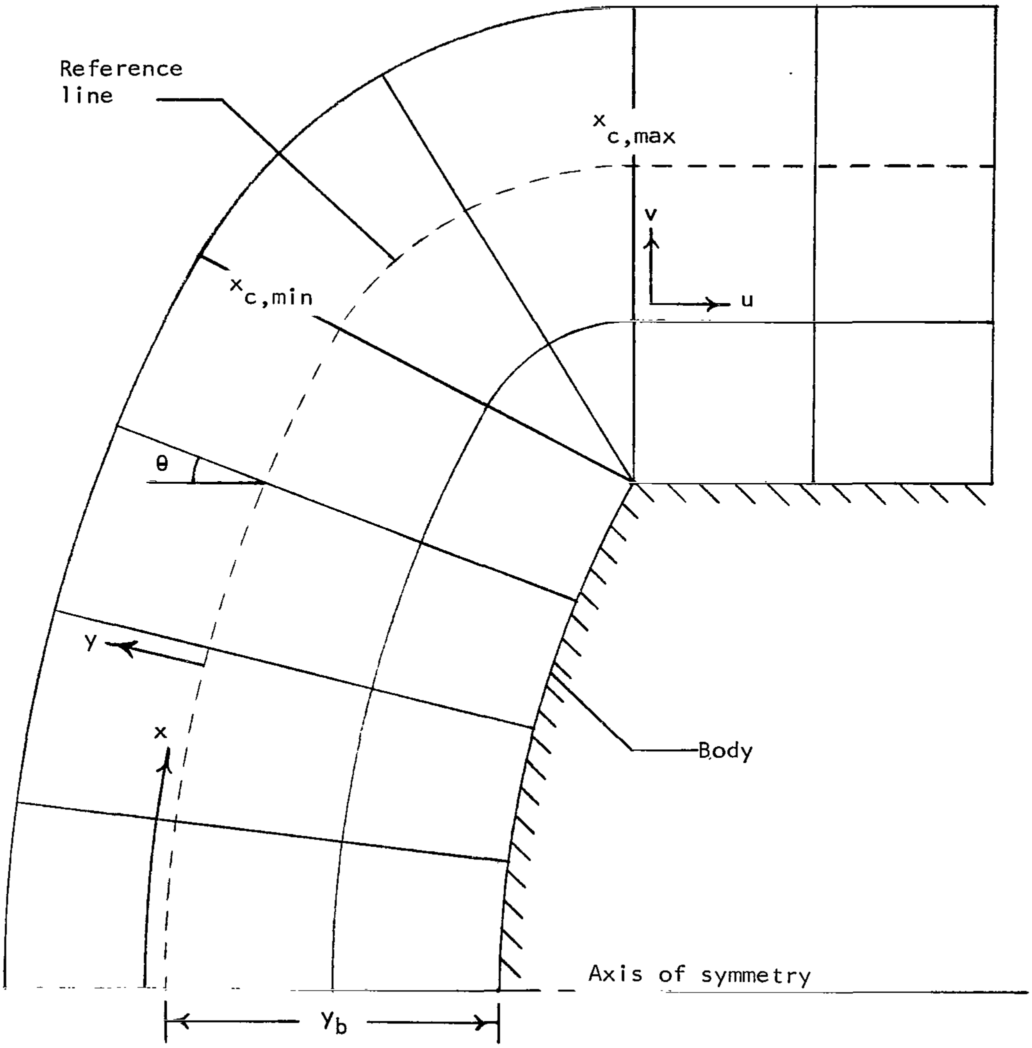

Figure 1.- Body-oriented coordinate system.

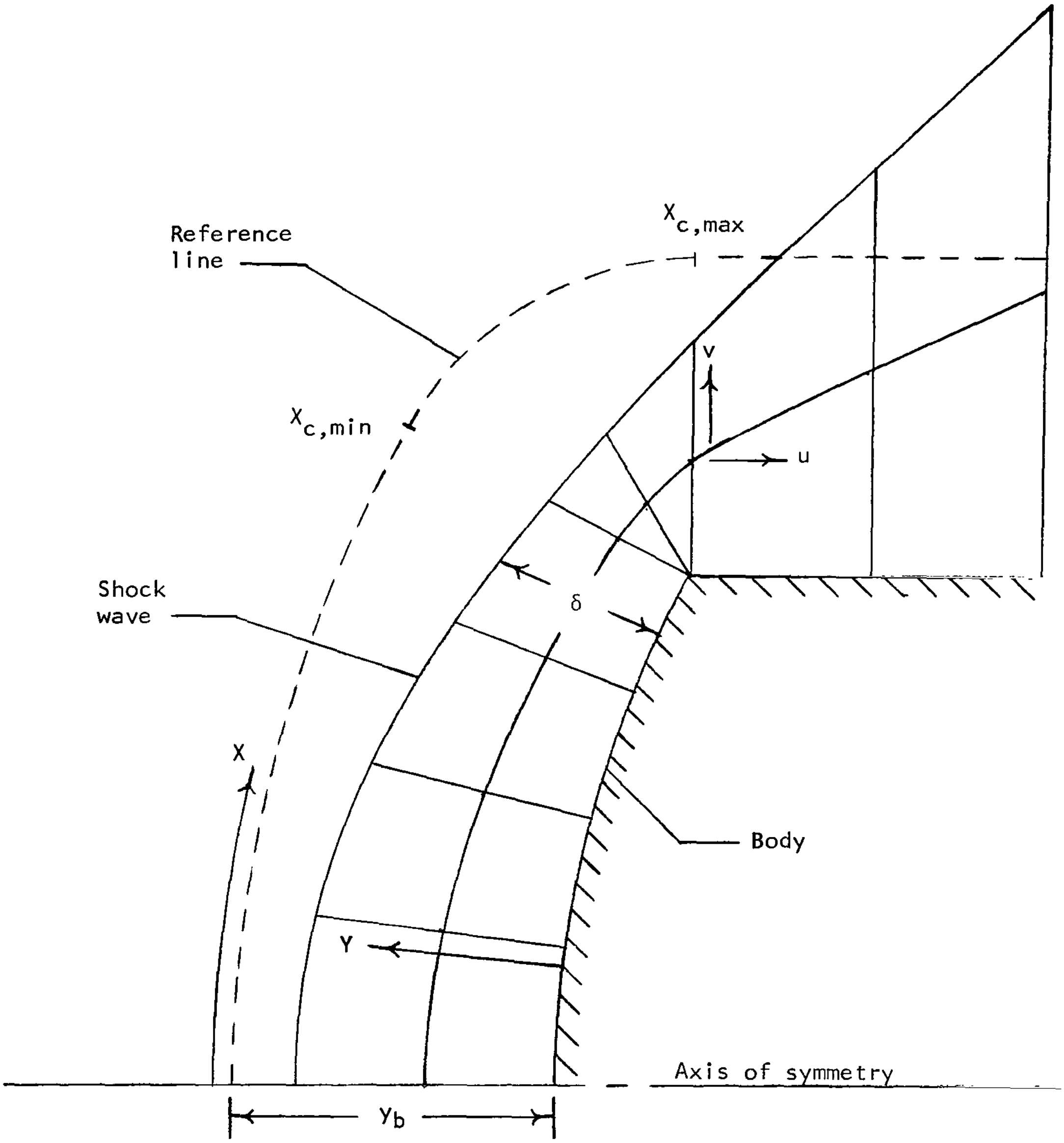

Figure 2.- Normalized coordinate system.

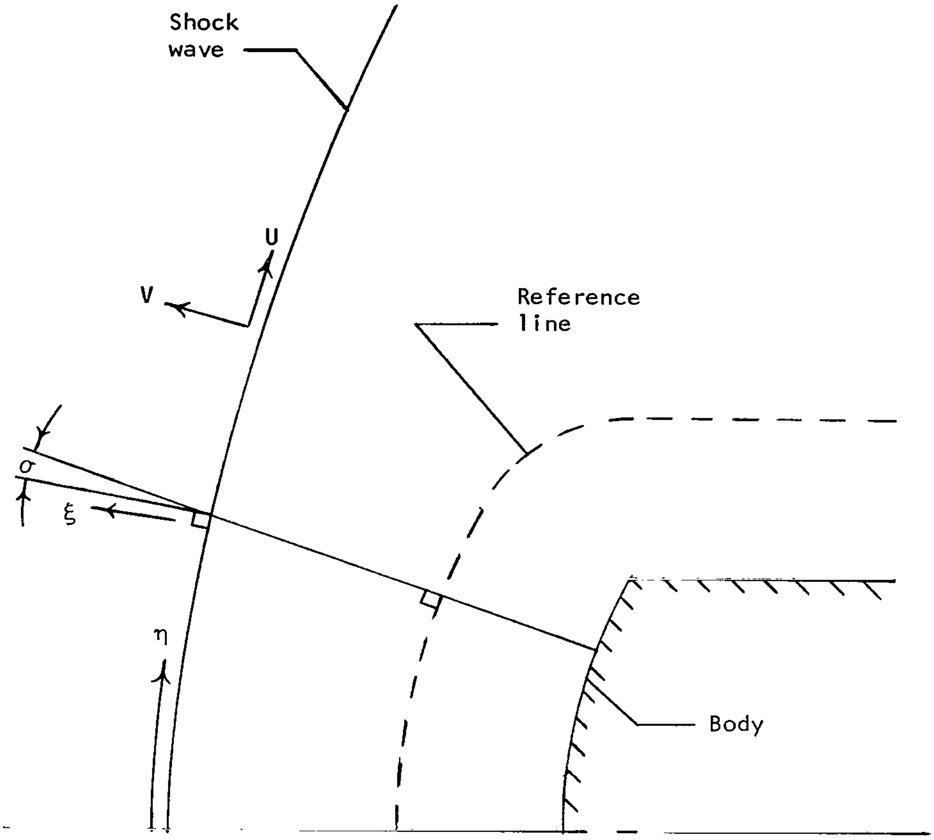

Figure 3.- Shock-oriented coordinate system.

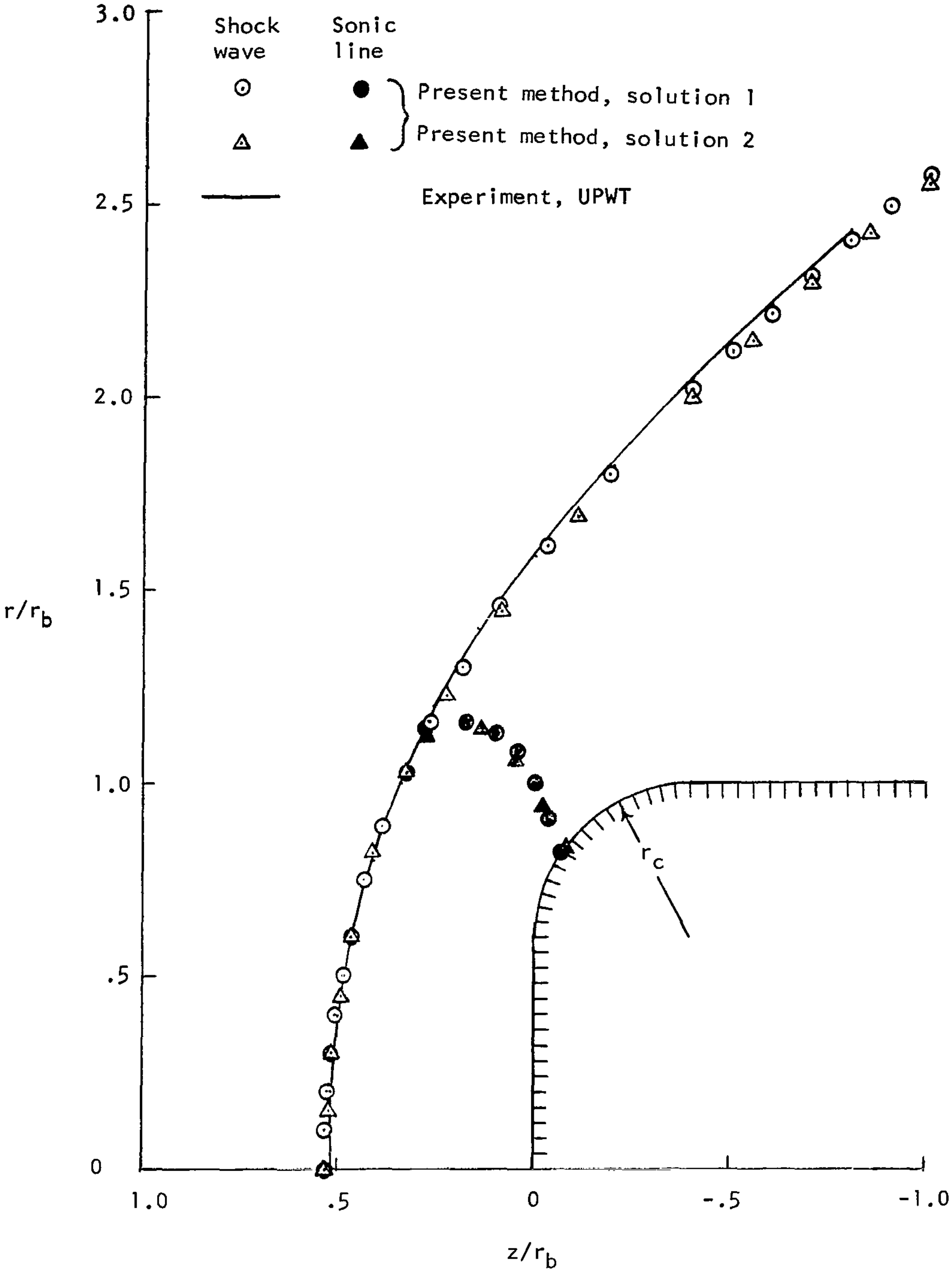

Figure 4.- Shock-wave and sonic-line locations for flat-face cylinder with $r_c/r_b = 0.4$. $\gamma = 1.4$; $M_\infty = 2.49$.

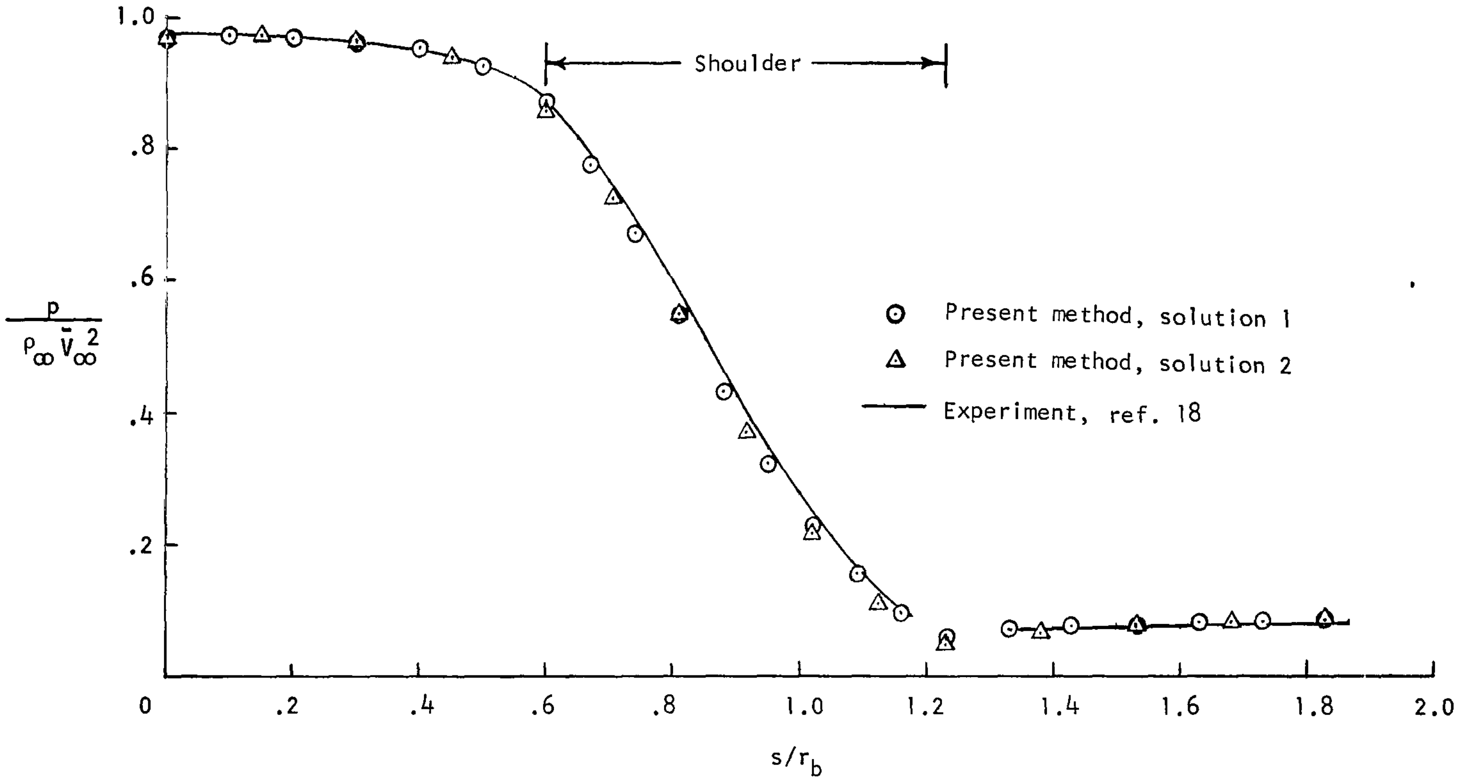

(a) Pressure distribution.

Figure 5.- Surface pressure and velocity distributions for flat-face cylinder with $r_c/r_b = 0.4$. $\gamma = 1.4$; $M_\infty = 2.49$.

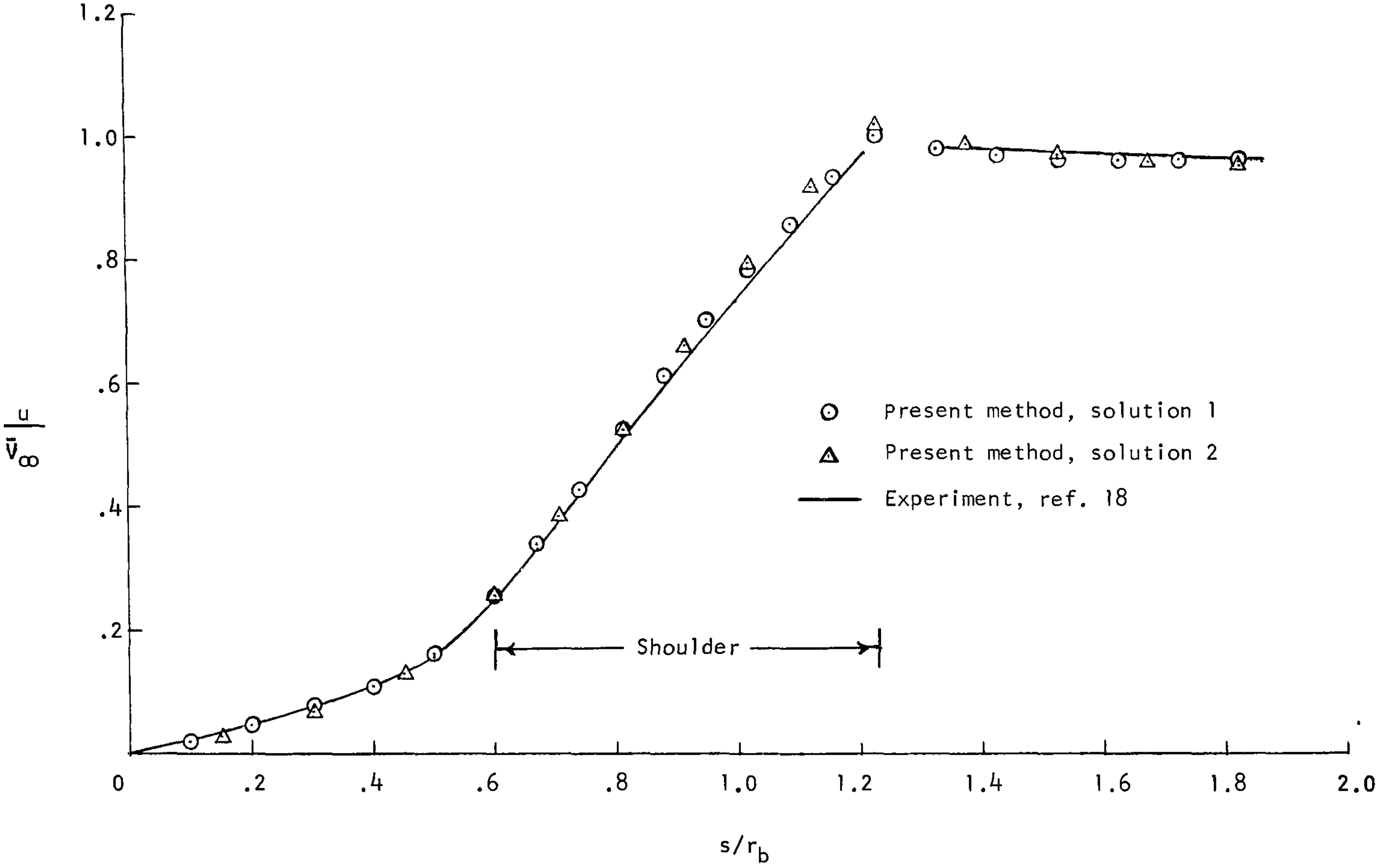

(b) Velocity distribution.

Figure 5.- Concluded.

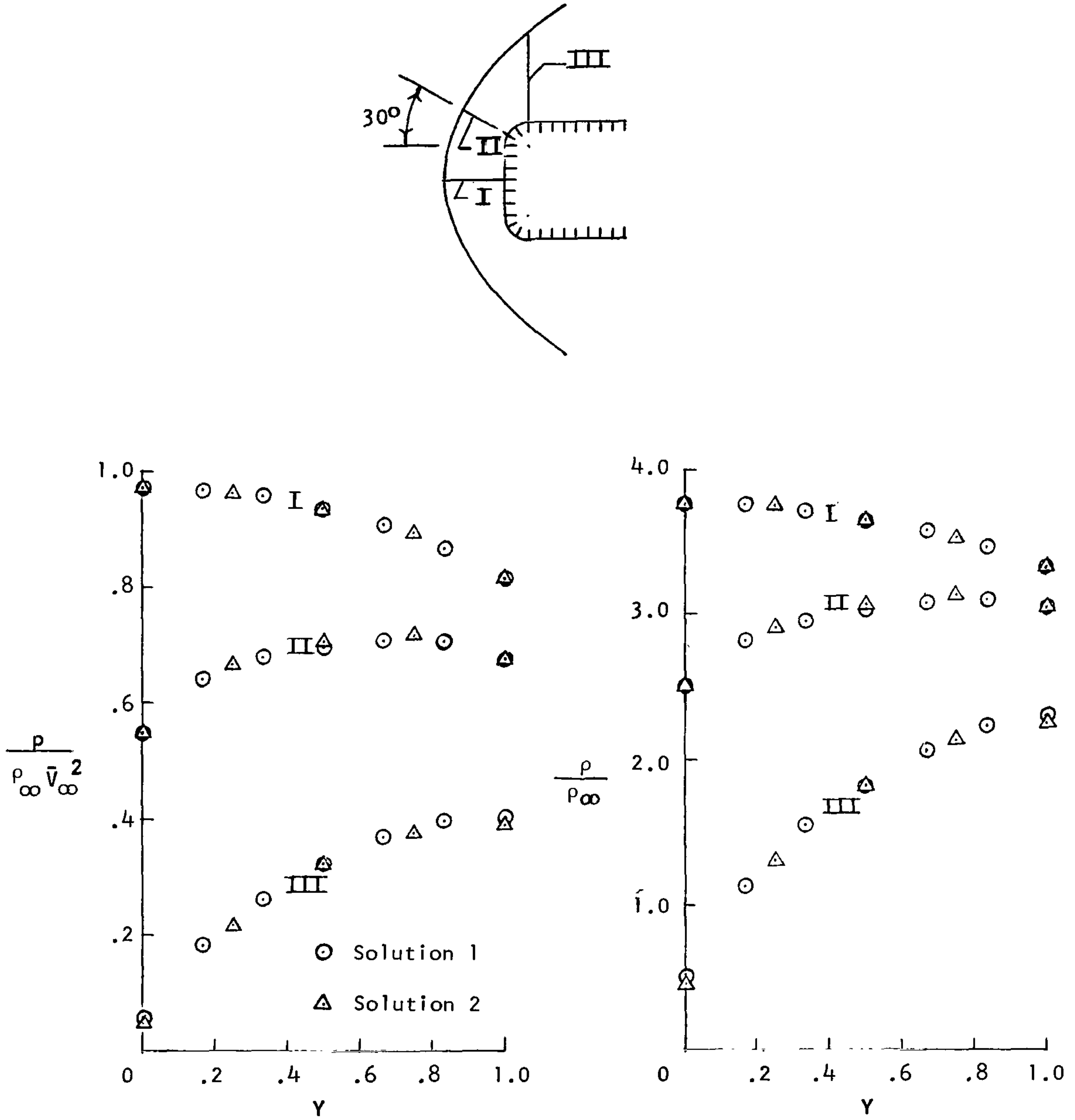

(a) Pressure.

(b) Density.

Figure 6.- Present results for distributions of flow properties across shock layer for flat-face cylinder with $r_c/r_b = 0.4$. $\gamma = 1.4$; $M_\infty = 2.49$. The coordinate Y has values of 1 and 0 at the shock wave and body surface, respectively.

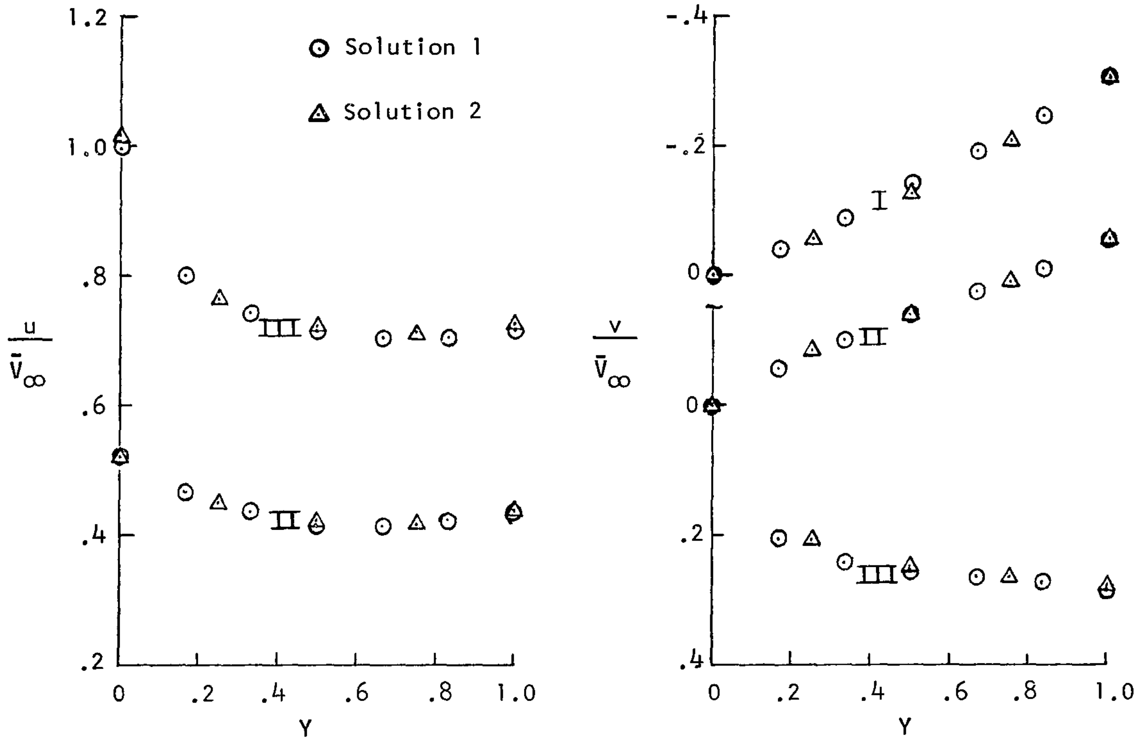

(c) Tangential velocity component.

(d) Normal velocity component.

Figure 6.- Concluded.

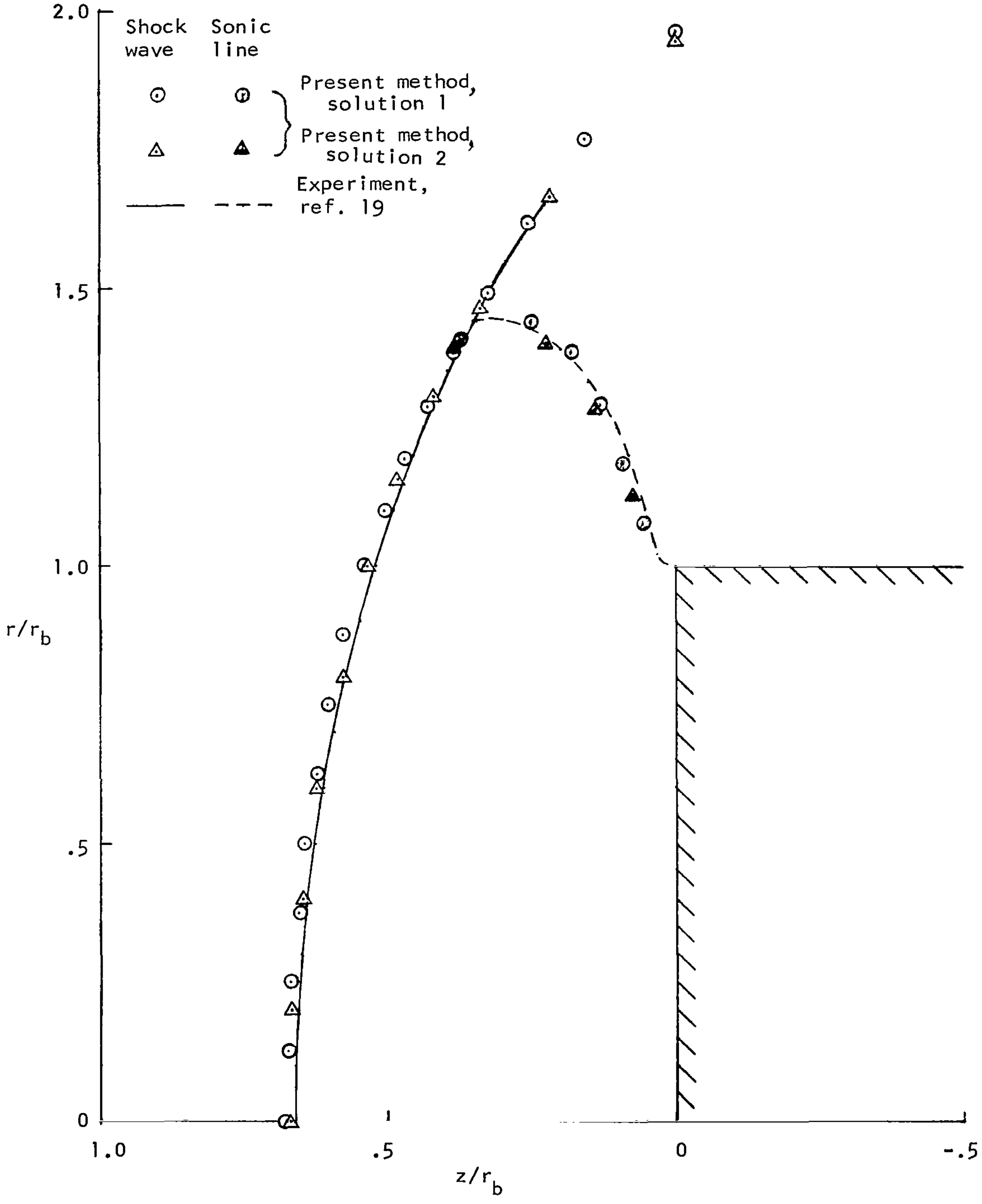

Figure 7.- Shock-wave and sonic-line locations for flat-face cylinder with sharp corner. $\gamma = 1.4$; $M_\infty = 2.81$.

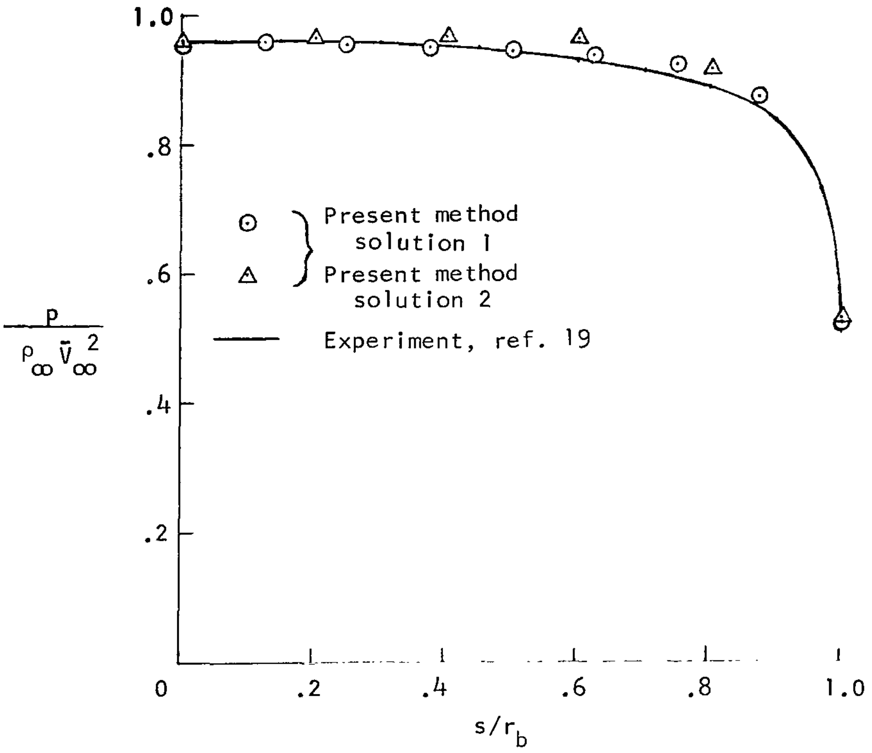

(a) Pressure distribution.

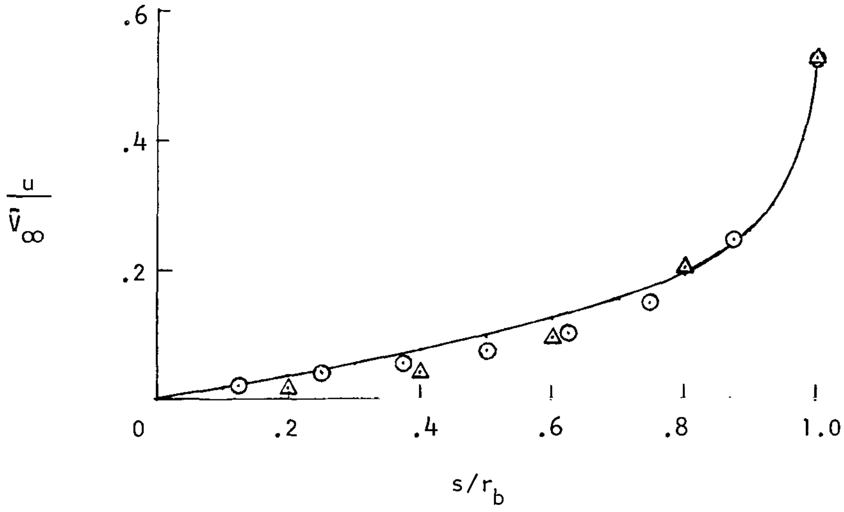

(b) Velocity distribution.

Figure 8.- Surface pressure and velocity distribution for flat-face cylinder with sharp corner. $\gamma = 1.4$; $M_\infty = 2.81$.

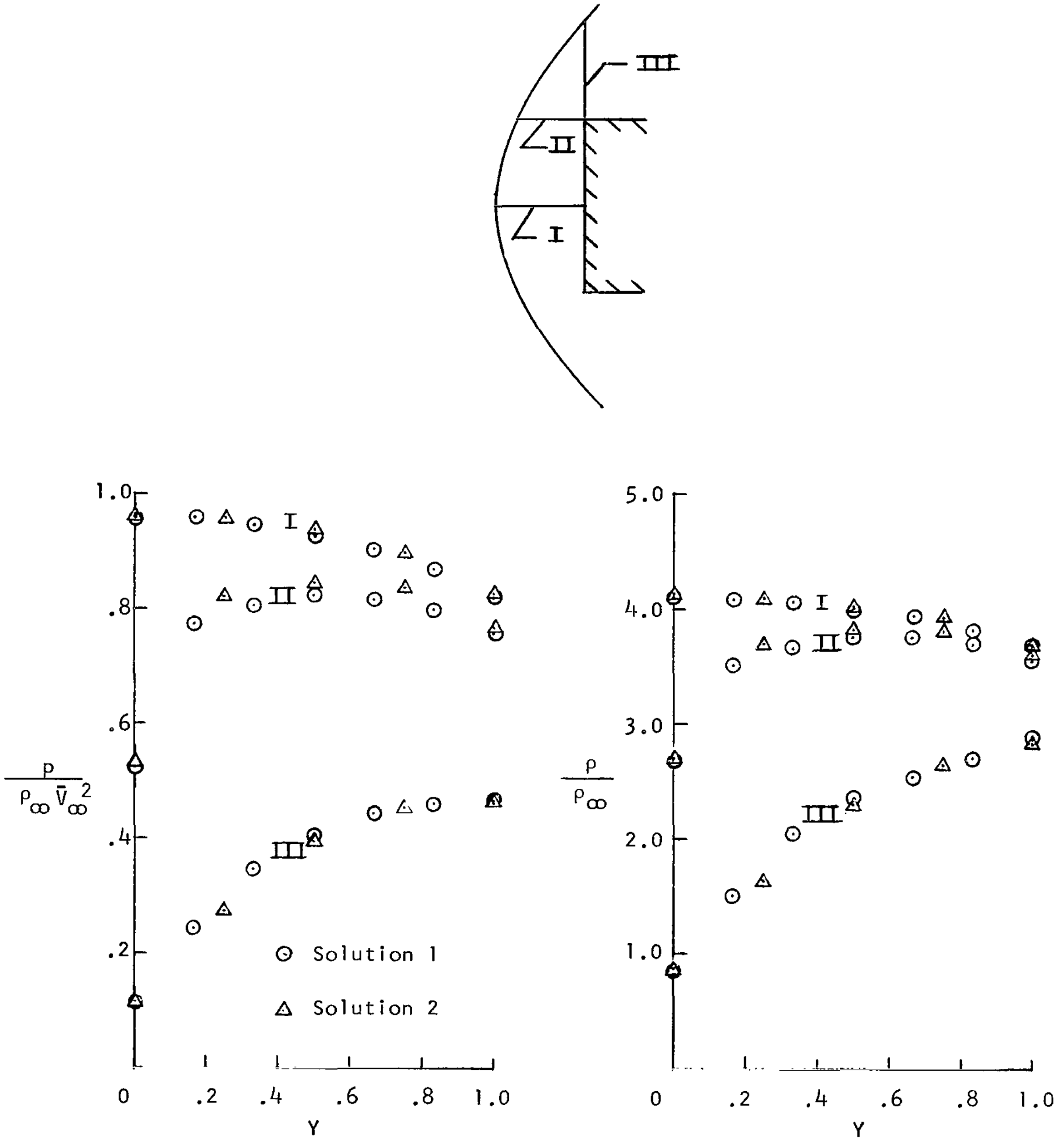

(a) Pressure.

(b) Density.

Figure 9.- Present results for distributions of flow properties across shock layer for flat-face cylinder with sharp corner. $\gamma = 1.4$; $M_\infty = 2.81$. The coordinate Y has values of 1 and 0 at the shock wave and body surface, respectively.

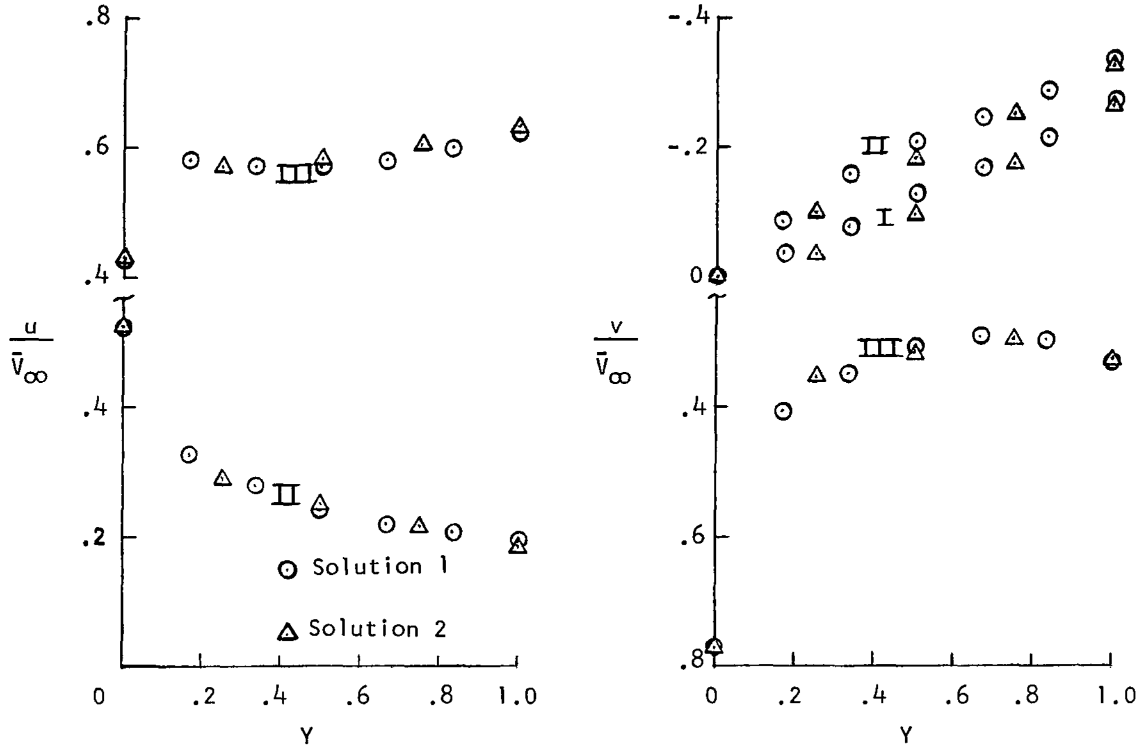

(c) Tangential velocity component.

(d) Normal velocity component.

Figure 9.- Concluded.

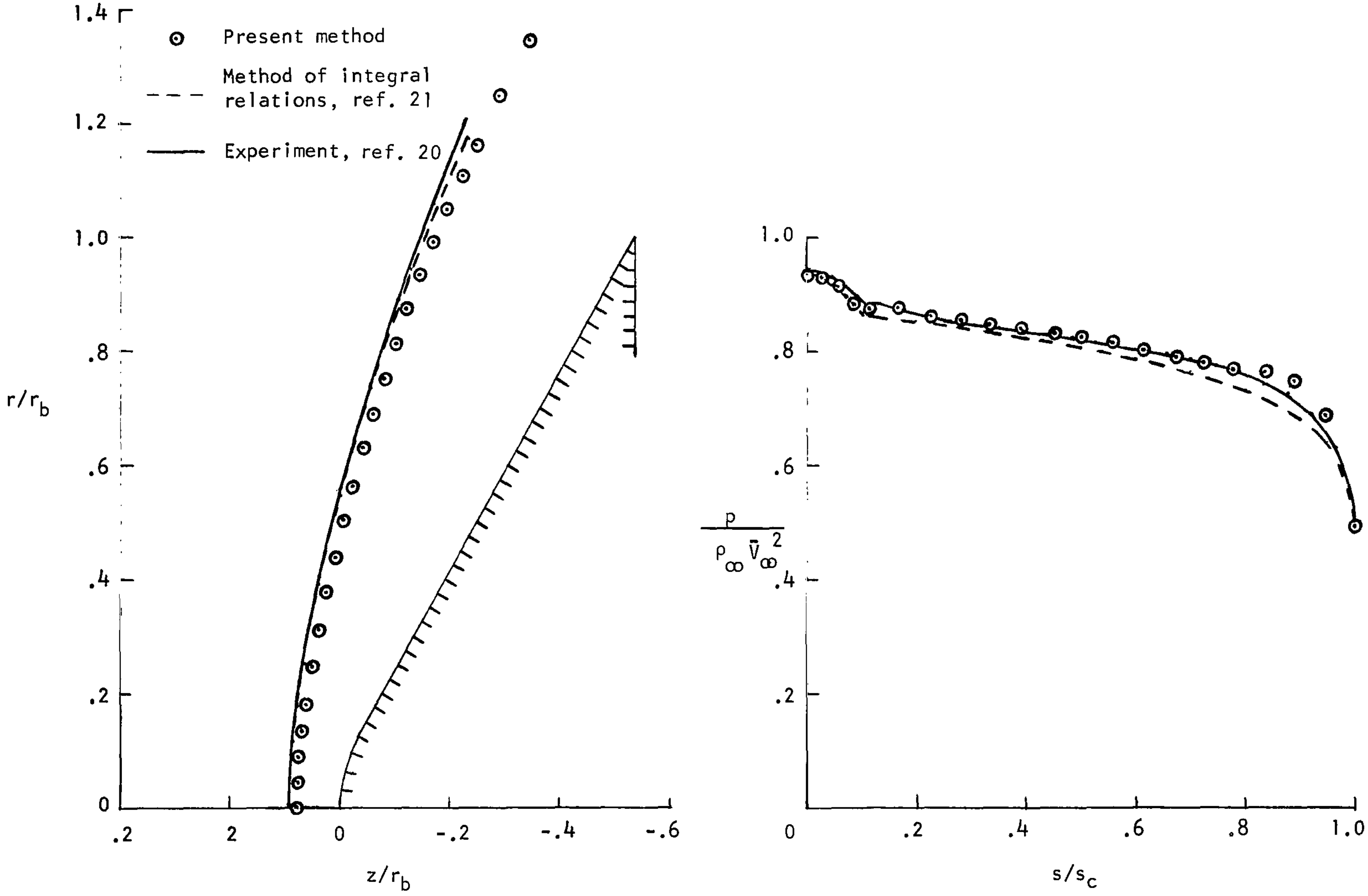

(a) Shock wave location.

(b) Surface pressure distribution.

Figure 10.- Comparison of results for spherically blunted 60° cone with $r_n/r_b = 0.25$. $\gamma = 1.4$; $M_\infty = 4.63$.

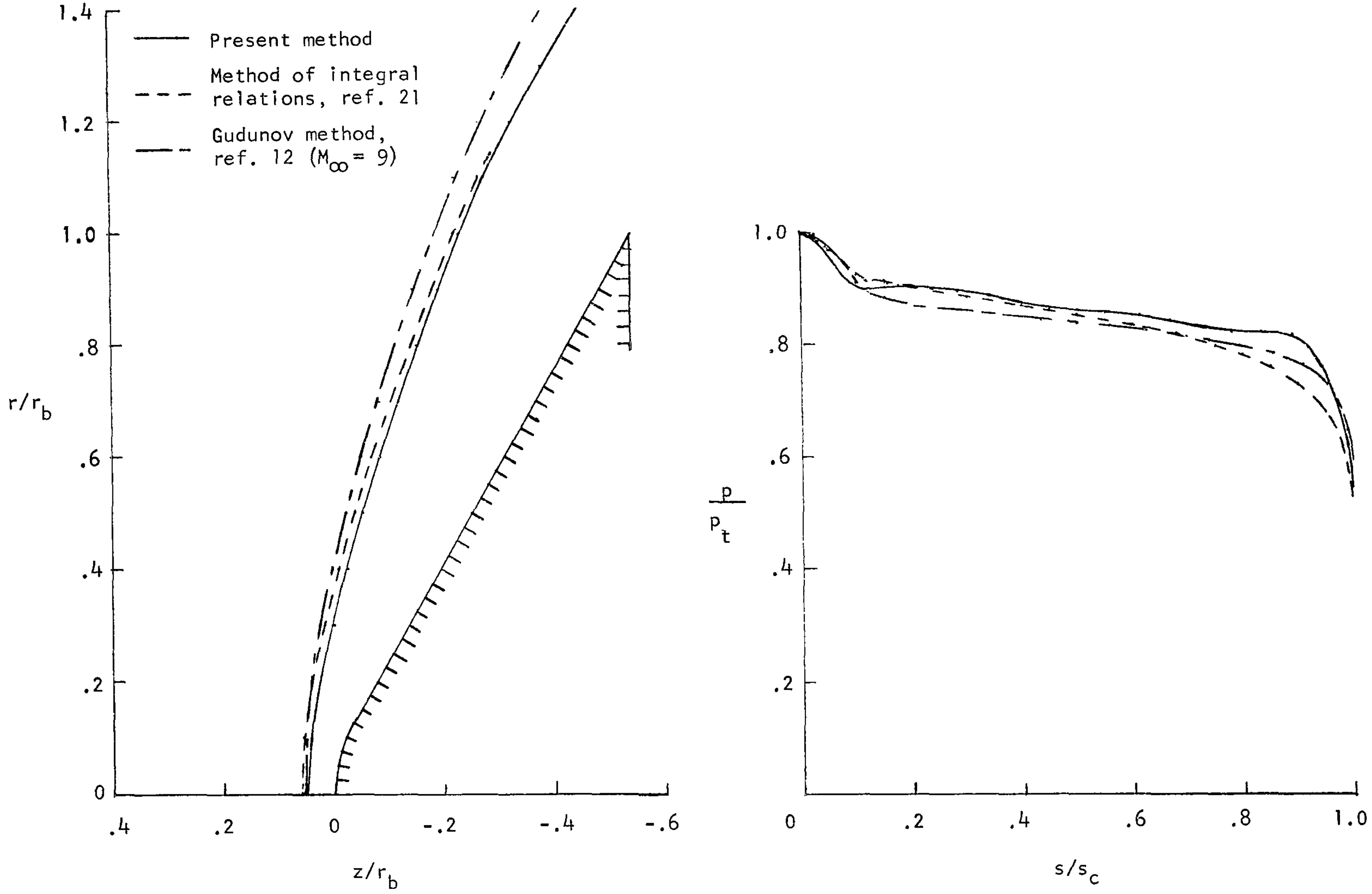

(a) Shock wave location.

(b) Surface pressure distribution.

Figure 11.- Comparison of results for spherically blunted 60° cone with $r_n/r_b$ = 0.25. $\gamma$ = 1.4; $M_\infty$ = 10 except as noted.

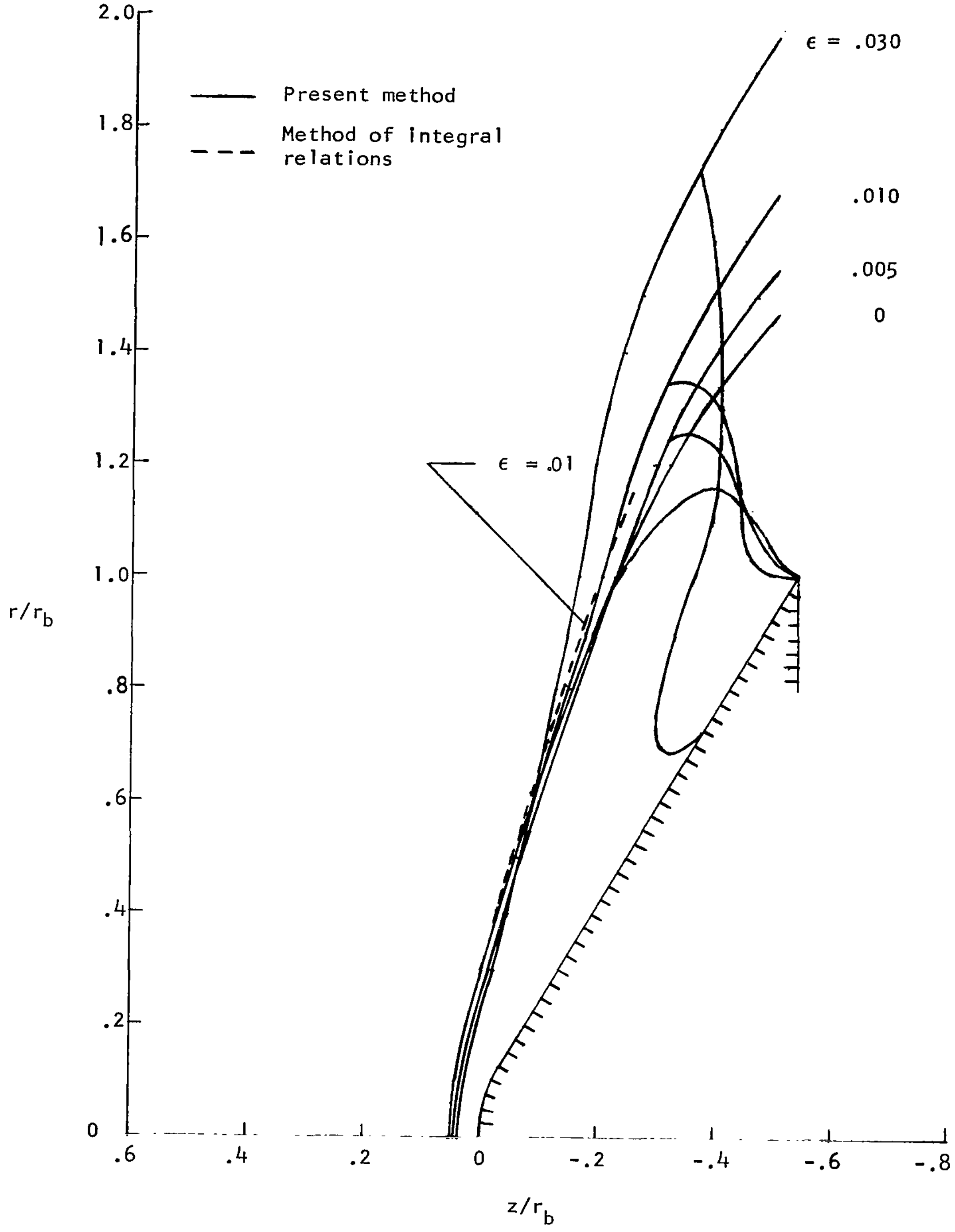

Figure 12.- Effect of parabolic free-stream velocity distribution on shock-wave and sonic-line locations for spherically blunted $60^{\circ}$ cone with $r_n/r_b = 0.25$. $\gamma = 1.4$; $M_{\infty,\mathrm{C\!\!\!L}} = 10$.

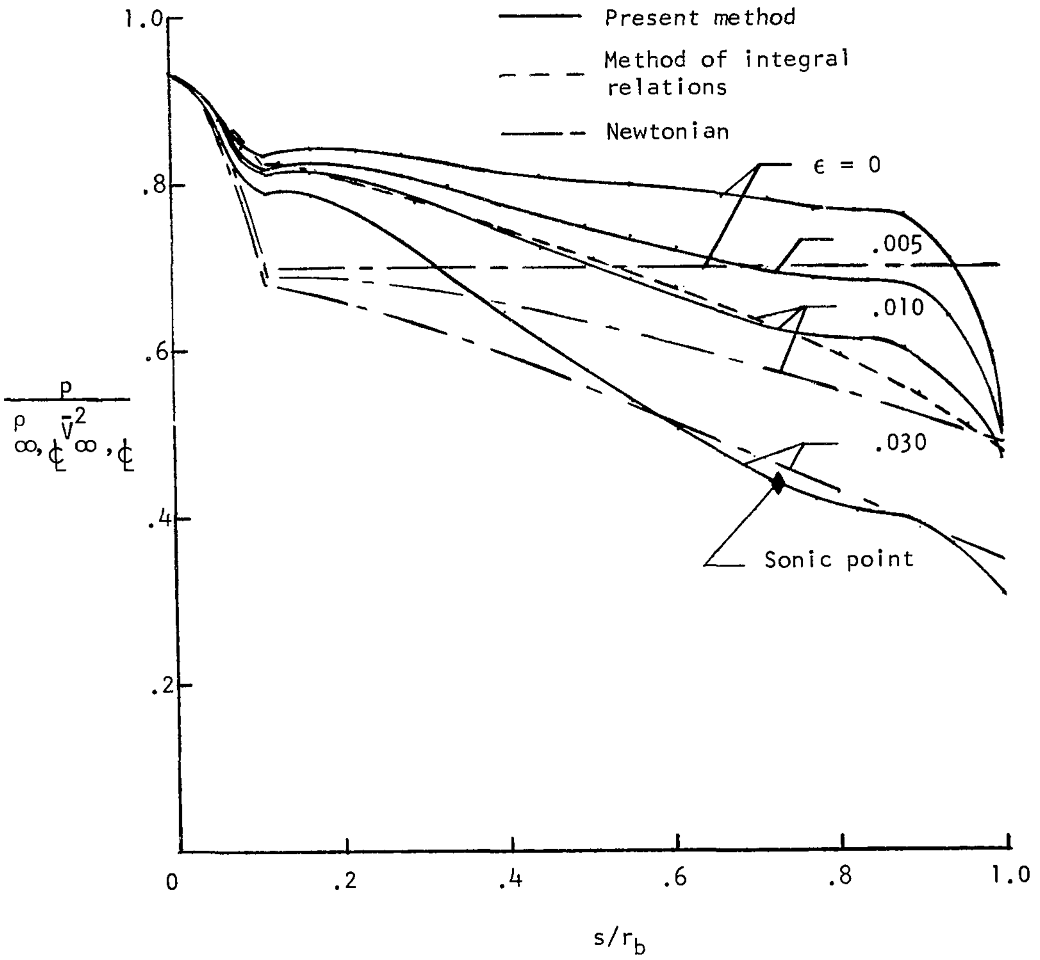

Figure 13.- Effect of parabolic free-stream velocity distribution on surface pressure distribution for spherically blunted 60° cone with $r_n/r_b = 0.25$. $\gamma = 1.4$; $M_{\infty,\mathrm{CL}} = 10$.

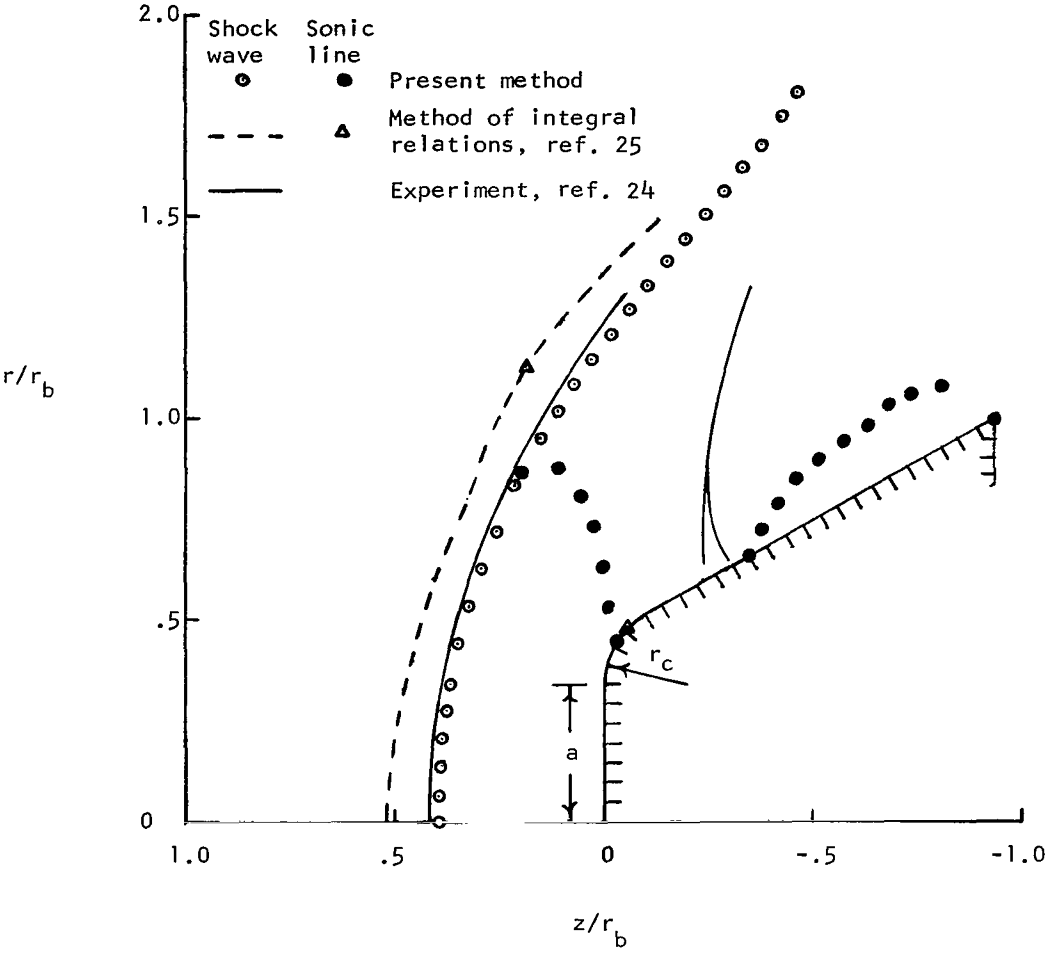

Figure 14.- Shock-wave and sonic-line locations for truncated $30^{\circ}$ cone with $a/r_b = 0.344$ and $r_c/r_b = 0.2$. $\gamma = 1.4$; $M_{\infty} = 1.79$.

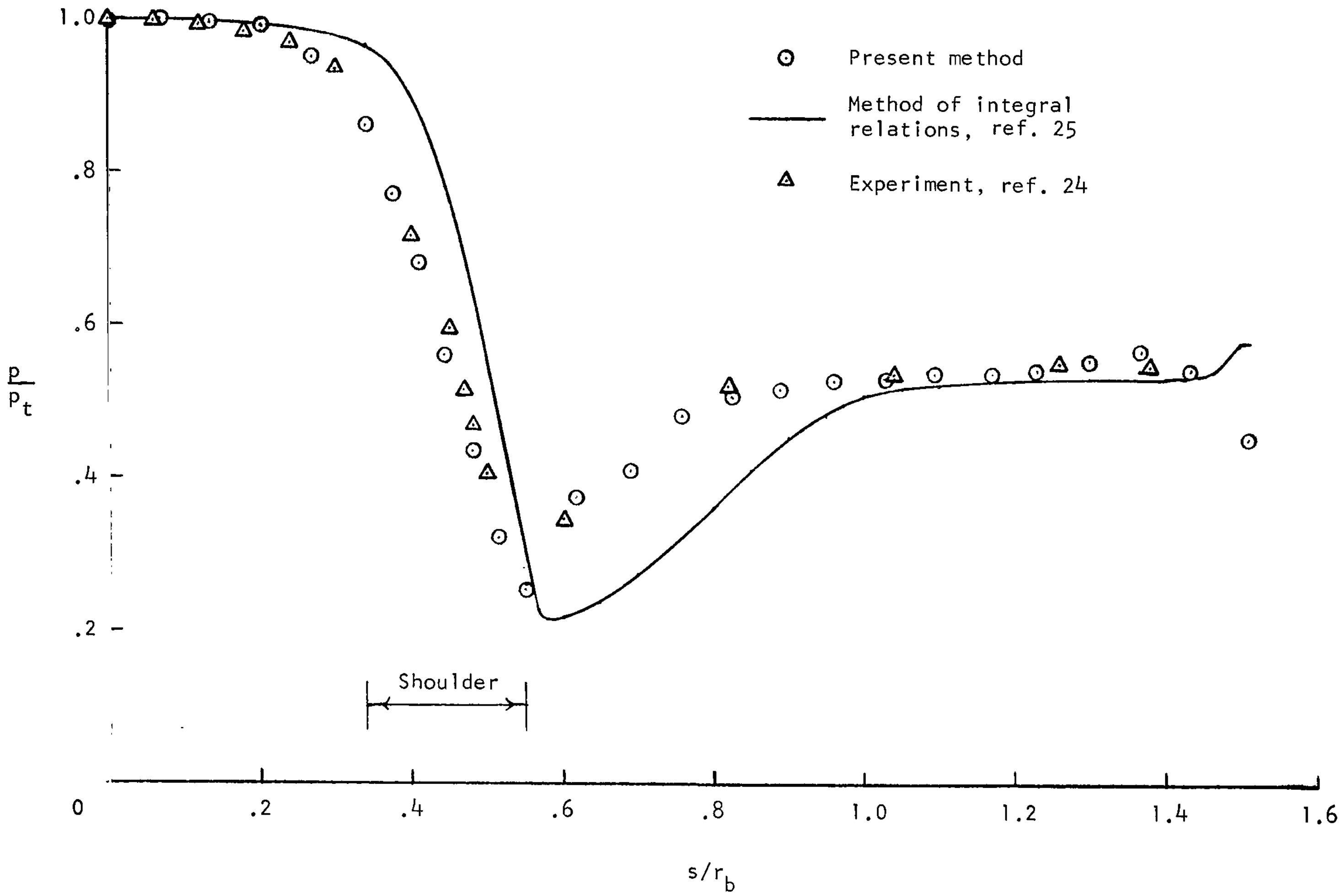

Figure 15.- Surface pressure distribution for truncated $30^\circ$ cone with $a/r_b = 0.344$ and $r_c/r_b = 0.2$. $\gamma = 1.4$; $M_\infty = 1.79$.

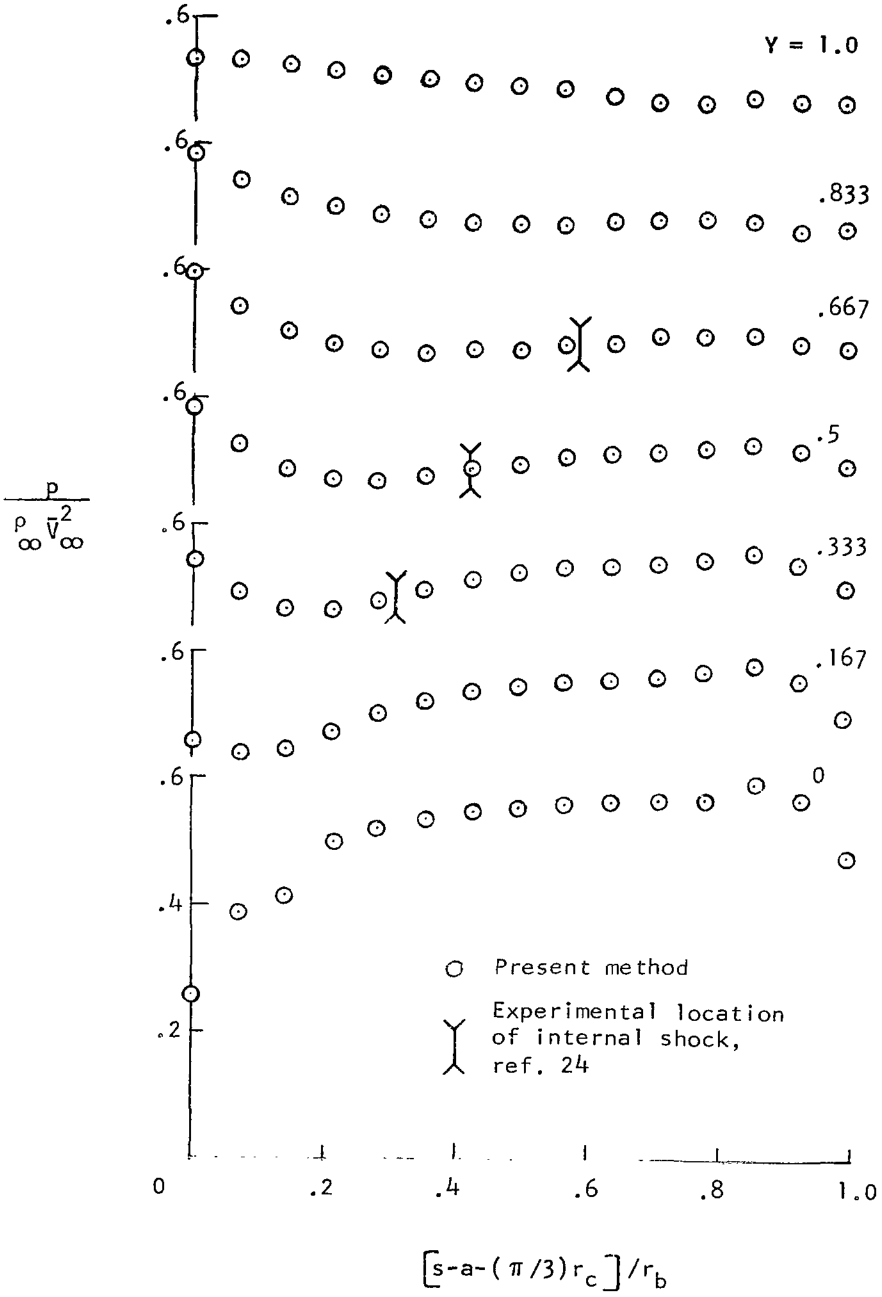

Figure 16.- Pressure distributions along lines of constant Y in vicinity of conical part of truncated 30° cone with $a/r_b = 0.344$ and $r_c/r_b = 0.2$. $\gamma = 1.4$; $M_\infty = 1.79$.

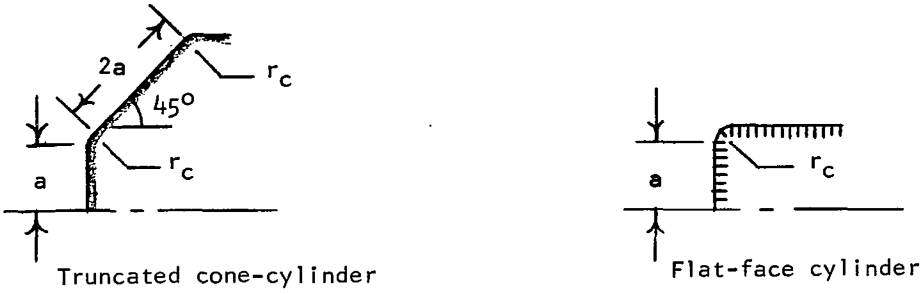

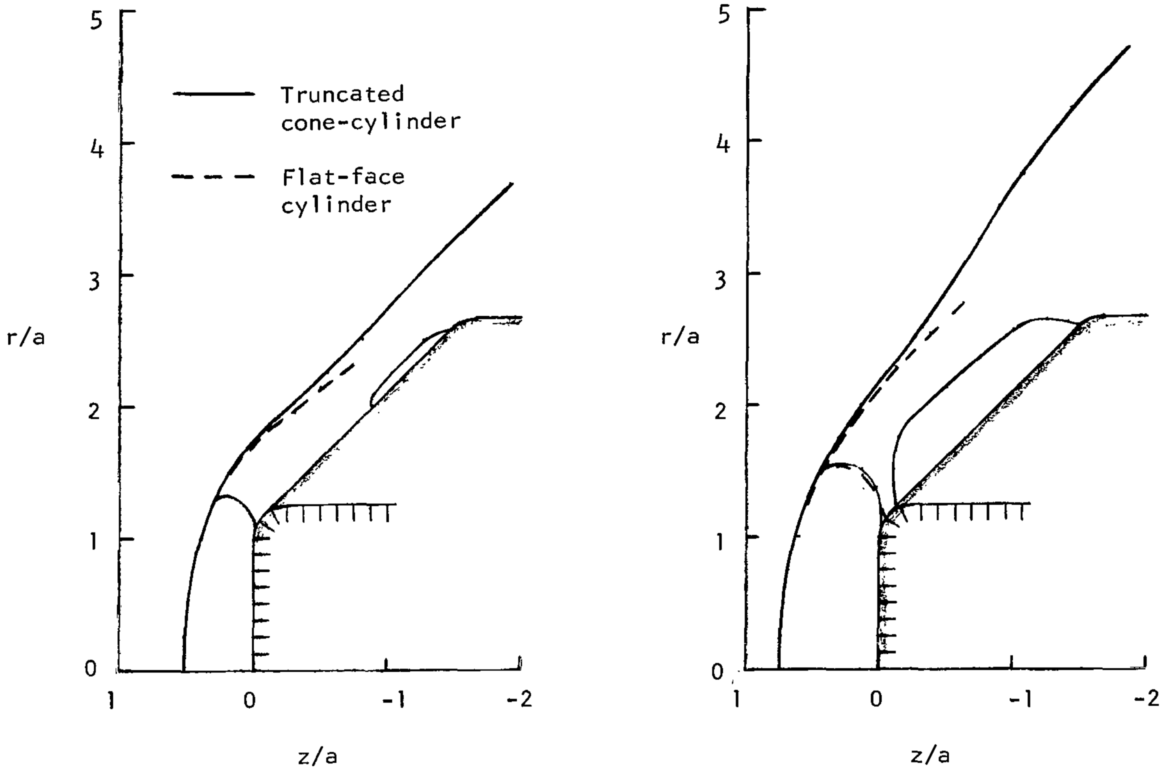

(a) $M_\infty = \infty$.

(b) $M_\infty = 2.8$.

Figure 17.- Effect of Mach number on shock-wave and sonic-line locations for truncated 45° cone and flat-face cylinder with $r_c/a = 0.25$. $\gamma = 1.4$.

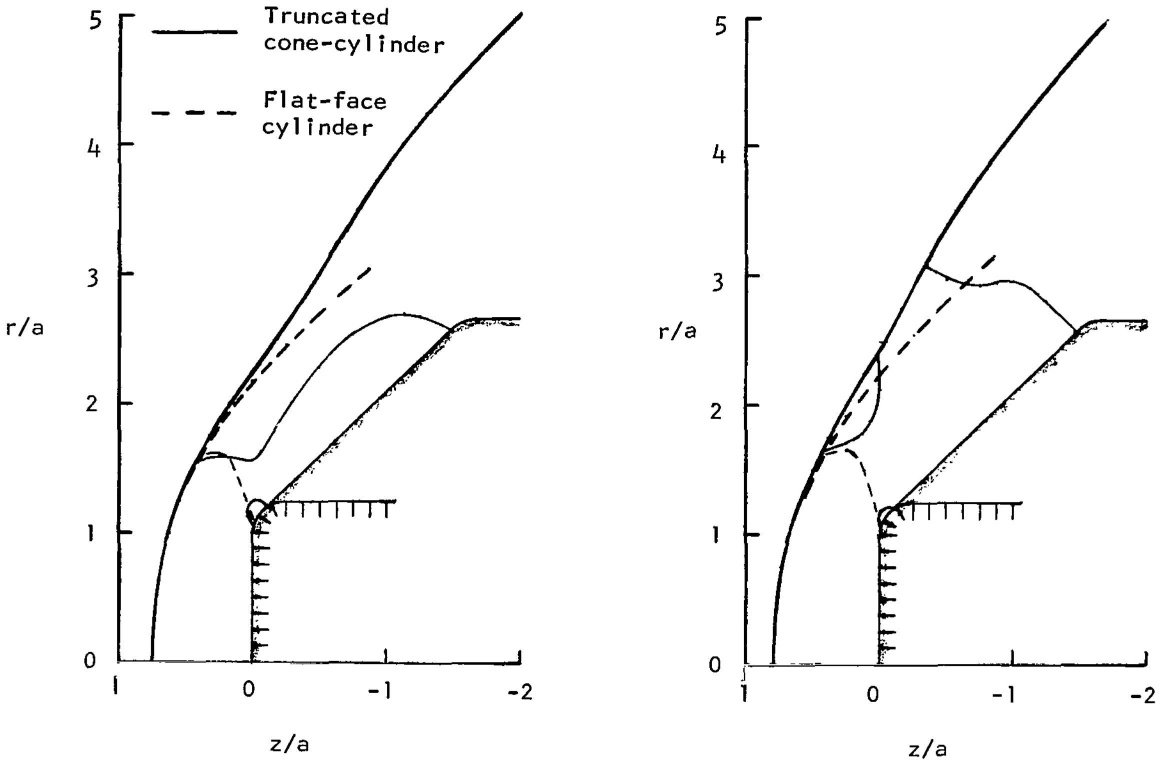

(c) $M_\infty = 2.6$.

(d) $M_\infty = 2.4$.

Figure 17.- Continued.

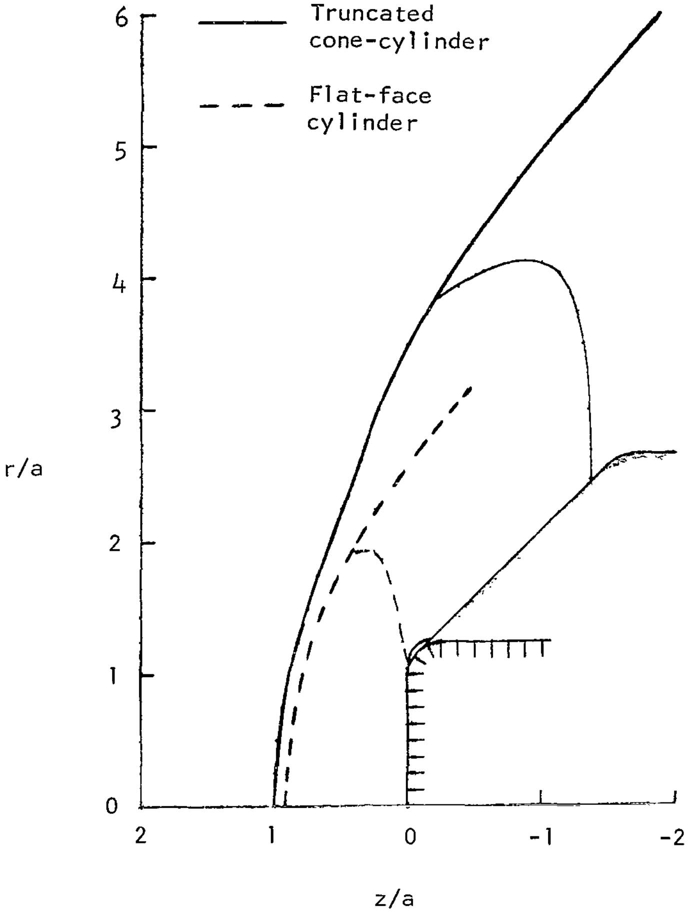

(e) $M_\infty = 2.0$.

Figure 17.- Concluded.

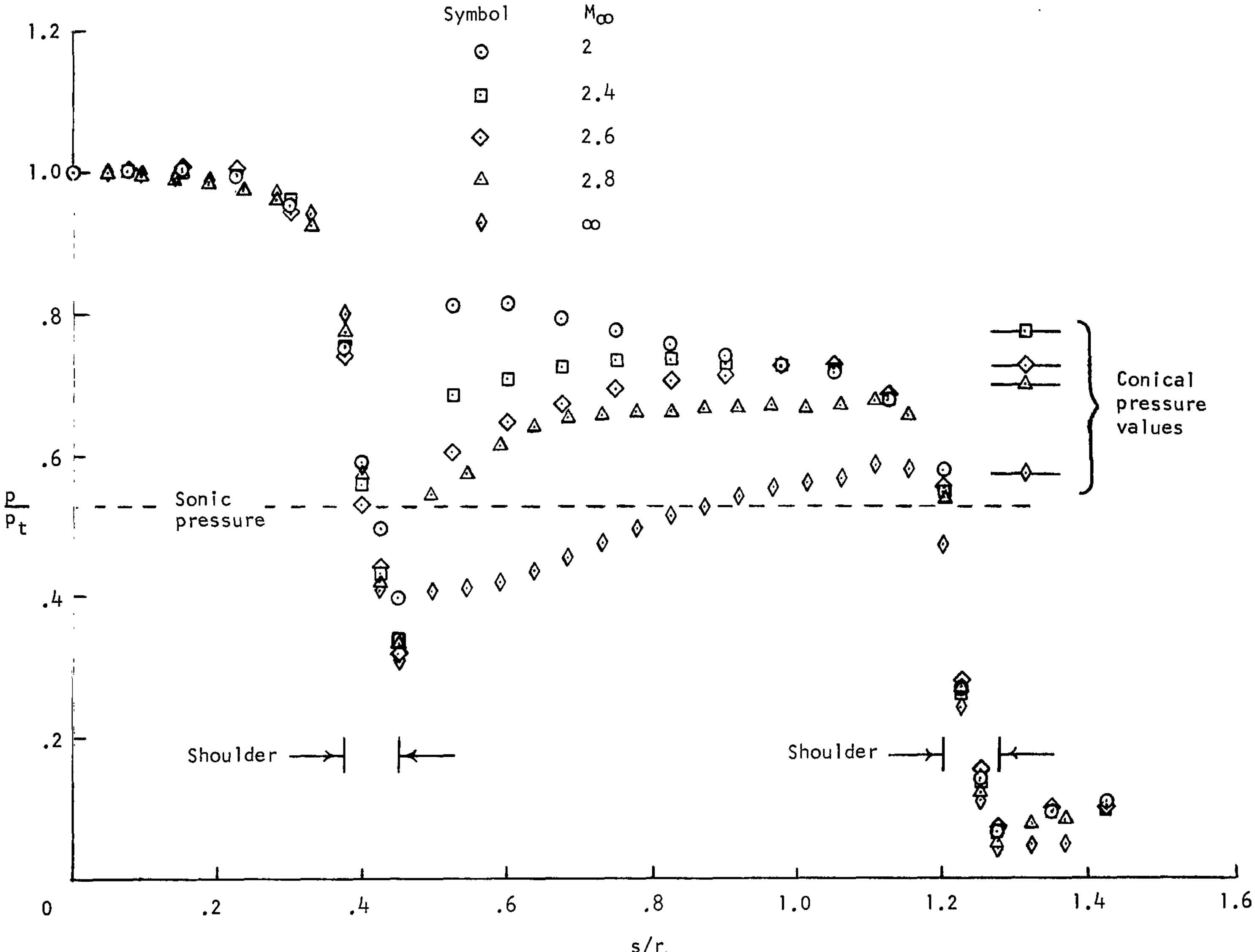

Figure 18.- Effect of Mach number on surface pressure distribution for truncated 45° cone with $r_c/a = 0.25$. $\gamma = 1.4$.

NATIONAL AERONAUTICS AND SPACE ADMINISTRATION
WASHINGTON, D. C. 20546

OFFICIAL BUSINESS

**FIRST CLASS MAIL**

POSTAGE AND FEES PAID
NATIONAL AERONAUTICS AND
SPACE ADMINISTRATION

06U 001 37 51 3DS 70316 00903
AIR FORCE WEAPONS LABORATORY /WLOL/
KIRTLAND AFB, NEW MEXICO 87117

ATT E. LOU BOWMAN, CHIEF,TECH. LIBRARY

POSTMASTER: If Undeliverable (Section 158 Postal Manual) Do Not Return

> *"The aeronautical and space activities of the United States shall be conducted so as to contribute . . . to the expansion of human knowledge of phenomena in the atmosphere and space. The Administration shall provide for the widest practicable and appropriate dissemination of information concerning its activities and the results thereof."*
>
> —NATIONAL AERONAUTICS AND SPACE ACT OF 1958

# NASA SCIENTIFIC AND TECHNICAL PUBLICATIONS

TECHNICAL REPORTS: Scientific and technical information considered important, complete, and a lasting contribution to existing knowledge.

TECHNICAL NOTES: Information less broad in scope but nevertheless of importance as a contribution to existing knowledge.

TECHNICAL MEMORANDUMS: Information receiving limited distribution because of preliminary data, security classification, or other reasons.

CONTRACTOR REPORTS: Scientific and technical information generated under a NASA contract or grant and considered an important contribution to existing knowledge.

TECHNICAL TRANSLATIONS: Information published in a foreign language considered to merit NASA distribution in English.

SPECIAL PUBLICATIONS: Information derived from or of value to NASA activities. Publications include conference proceedings, monographs, data compilations, handbooks, sourcebooks, and special bibliographies.

TECHNOLOGY UTILIZATION PUBLICATIONS: Information on technology used by NASA that may be of particular interest in commercial and other non-aerospace applications. Publications include Tech Briefs, Technology Utilization Reports and Notes, and Technology Surveys.

*Details on the availability of these publications may be obtained from:*

**SCIENTIFIC AND TECHNICAL INFORMATION DIVISION**

**NATIONAL AERONAUTICS AND SPACE ADMINISTRATION**

**Washington, D.C. 20546**